Construction of Polyelectrolyte Microcapsules envisaging potential Cancer Therapy

Nuno Guilherme Branco Neto

Thesis to obtain the Master of Science Degree in

Bioengineering and Nanosystems

Supervisor: Doctor Suzana Maria de Andrade Sousa Paiva

Co-Supervisor: Doctor Vanda Isabel Roldão Vaz Serra

Examination Committee

Chairperson: Professor Gabriel António Amaro Monteiro

Co-Supervisor: Doctor Vanda Isabel Roldão Vaz Serra

Members of the Commitee: Doctor Joana Filipa Brites Barata

November of 2017

Resumo

Esta tese propõe um novo sistema de transporte de porfirinoídes, de modo a aumentar a eficiência da terapia fotodinâmica com a possibilidade de rastreamento (por emissão de luz) para terapia de cancro. Duas porfirinas diferentes: uma carregada negativamente, 5,10,15,20-(tetrakis)-(4-sulfonatofenil) porfirina (H_2TSPP^{-4}) e uma carregada positivamente, 5,10,15,20-(tetrakis)-(N-metil-4-piridinium-il) porpfirina (TMPyP) foram usadas como fotossensiblizadores e adsorvidas em microcápsulas com núcleo e com polielectrólitos sensíveis ao pH (PECs) de poli(estirenosulfonato) (PSS) e poli (hidrocloreto de alilamina) (PAH). A caracterização do sistema PEC foi realizada por absorção UV-Vis, emissão de fluorescência em estado estacionário e resolvida no tempo, microscopia de imagem de fluorescência resolvida no tempo, potencial zeta e microscopia de transmissão eletrónica. As principais características deste sistema de transporte são uma libertação elevada da carga (87,7%) em ambientes de pH ácido (~ 3,0), uma elevada estabilidade com baixa libertação da carga (2,18%) em ambientes de pH neutro e não-degradação do sistema por efeito da luz em ambientes não-oxidativos. Também é relatada a formação organizada de H_4TSPP^{-2} em PECs em que o núcleo de $CaCO_3$ funciona como um local de nucleação para a formação de estruturas de agulha radialmente distribuídas de agregados de porfirina. Estes últimos resultados foram publicados no dia 11 de julho de 2017 em *Langmuir (Publicações da ACS)*.

Palavras-Chave: Microcápsulas, Porfirinas, Terapia Fotodinâmica, Polielectrólitos

Abstract

This thesis proposes a new porphyrinoid delivery system in order to increase the photodynamic efficiency with the possibility of light-tracking for Cancer therapy. Two different porphyrins: a negatively charged 5,10,15,20-(tetrakis)-(4-sulfonatophenyl) porphyrin (H_2TSPP^{-4}) and a positively charged 5,10,15,20-(tetrakis)-(N-methyl-4-pyridinium-yl) porphyrin (TMPyP) were used as photosensitizers and adsorbed in pH-sensitive core-shell polyelectrolyte microcapsules (PECs) of poly(styrenesulfonate) (PSS) and poly(allylamine hydrochloride) (PAH). The characterization of the PECs system was made by UV-Vis absorption, steady state and transient spectroscopy, Fluorescence Lifetime Imaging Microscopy (FLIM), zeta potential and Transmission Electron Microscopy (TEM). The key characteristics of this delivery system are: pH dependence on encapsulation efficiency; a high load release (87.7%) in acidic pH (~3.0) environments; a high stability with very low release (2.18%) in neutral pH environments and non-degradation of the system by light in non-oxidative environments. It is also reported the organized self-assembly of H_4TSPP^{-2} on PECs where the $CaCO_3$ core works as a nucleation site for the formation of radially distributed needle-like structures of porphyrin aggregates. These last results were published on 11th July of 2017 in *Langmuir (ACS Publications).*

Keywords: Microcapsules, Porphyrins, Photodynamic Therapy, Polyelectrolytes

General Index

List of Tables

List of Figures

List of Abbreviations

H_2TSPP^{-4} – 5,10,15,20-(tetrakis)-(4-sulfonatophenyl) porphyrin

TMPyP – 5,10,15,20-(tetrakis)-(N-methyl-4-pyridinium-yl) porphyrin

PECs – Polyelectrolyte Capsules

PSS – Poly(styrenesulfonate)

PAH – Poly(allylamine hydrochloride)

FLIM – Fluorescence Lifetime Image Microscopy

WHO – World Health Organization

PDT – Photodynamic Therapy

ROS – Reactive oxygen species

RNS – Reactive nitrogen species

LbL – Layer-by-Layer

CHAPTER 1

Introduction

According to a study from World Health Organization (WHO) in 2012, cancer is responsible for over eight million deaths and more than fourteen million new cancer cases were detected adding to thirty-two million people already living with cancer worldwide. Still, these numbers can have a tendency to increase. The International Agency for Research in Cancer reported that by 2035 over twenty-three million people should develop cancer and the death toll can increase up to fourteen million people [1]. This increase in incidence and mortality brings a focus to this problematic and a need to develop new therapeutics or improve current ones.

The current cancer treatments are very limited. The options available are usually surgery or chemotherapy. Surgery implies removal of tissue or organ infected imposing a physical trauma to the patient which is not always applicable or successful due metastasized cancers. Chemotherapy is the major therapeutic approach for the treatment of localized and metastasized cancers with the use of chemical drugs, mostly intravenously administered. These drugs normally show limitations in: specificity, selectivity, therapeutic index, solubility and stability. Other limitations include: induction of chemo-resistance and low molecular weight [2].

Previous limits might be overcome by using polyelectrolyte microcapsules as a delivery system of a therapeutic drug.

These engineered micro-carriers offer advantages towards drug delivery, such as high loading/release of several drugs (as photosensitizer used in PDT), surface characteristics feasible for specific targeting, protection of drugs enhancing their stability, minimize their systemic clearance and also structural characteristics that enable their compartmentalization providing an easy way to incorporate different drugs and simultaneous therapeutics.

The polyelectrolyte microcapsule properties drive the pharmacokinetics, the pharmacodynamics and the biodistribution of the entire system in vivo. Altering parameters such as size, conformation and surface can result in alterations regarding the interaction between the carrier and the biological environment [3,4].

a. Photodynamic Therapy

The basis of PDT incurs in the use of photosensitizers, an adequate source of light (specific wavelength) and the oxygen dissolved in the target tissue [5] ending with the formation of reactive oxygen species (ROS) and reactive nitrogen species (RNS), which are active molecules that are harmful for a normal function of the organism. These molecules can also be formed during physiological processes but extremely high levels of these molecules can appear with the development of certain diseases [6].

When the concentration of antioxidants is low and a high level of free reactive species is present, the organism (and its cells) will suffer oxidative stress which can lead to cell damage, DNA mutation and numerous diseases [7]. Due to the high reactivity of oxygen species which are formed in the presence of photosensitizer, special attention has been given towards the development of new photosensitizers for therapeutic applications such as PDT. This therapy can be divided in two types (I and II) according to the amount of oxygen available in the tissue.In type I, there is a low concentration of oxygen in the

cell, the triplet excited state of the photosensitizer reacts with the tissue forming new radicals that react rapidly with oxygen present in the environment, leading to the formation of ROS (H_2O_2). In type II, there is a high oxygen concentration, the excited photosensitizer in the triplet state transfers energy to the triplet oxygen leading to singlet oxygen generation [1]. Type II refers to the conditions in which our study applies.

The PDT has potential advantages comparing with conventional cancer therapies, there are: Non-Invasive; Can be target accurately and selectively in early or localized cancer; It can improve quality of life and lengthen survival (in case of advanced disseminated disease); Repeated doses can be given without total-dose limitation; has less side-effects; it doesn't scar tissue; can be implemented with low infrastructures investments [8].

Cancer cells have a high supply of blood and a weak lymphatic drain which provides a high concentration of photosensitizers in this type of tissues comparing to the normal healthy tissue. This selectivity for cancer cells provides a higher generation of reactive oxygen species which improves the photodynamic efficiency [8].

One of the key components for PDT is the photosensitizer. It should be characterized by high chemical purity, activation wavelength adequate for tissue penetration, selectivity for tumor cells and formation of a long-lived triplet excited state. The most important factors are the period of photosensitivity, availability, concentration and the activation wavelength [9].

b. Light Absorption and Excited state deactivation pathways

As PDT is a process that starts with light absorption by the photosensitizer, it is important to study the physical-chemical pathways involved in the deactivation of its excited states.

The photosensitizes, as the name indicates are sensitive to light (photons) and, as already has been stated, there is a need of a source of light at a certain wavelength to "activate" the photosensitizer that transfers energy to molecular oxygen with the formation of reactive oxygen species that interact with the cancer tissue.

After light absorption, the molecule is excited to higher vibrational levels such as S_1 or S_2. the fluorophore undergoes an internal conversion process of relaxation from S_2 to S_1 occurring prior to fluorescence emission (figure 1). From the lowest energy vibrational state S_1, the fluorophore can relax to a ground state energy level accompanied by an emission of fluorescence. The fluorescence processes always occur from the lower vibrational level of S_1 as defined by Kasha rule [10]. The electronic excitations do not change the nuclear geometry so the spacing between the vibrational levels of the excited states and the ground state are similar originating a mirror-image between the emission and absorption spectrum. The absorption spectrum of a fluorophore shows distinct peaks resulting from different transitions to different vibrational energy levels. As a result, if a particular transition probability is allowed in absorption, the reciprocal transition is also most probable in emission.

The molecules in the S_1 state can undergo intersystem crossing to first triplet state T_1 (figure 1). Although this transition can occur, it is normally a forbidden transition between energy states of different multiplicity since the enhancement of spin-orbit coupling due to the presence of heavy atoms (metals

and halogens) can be facilitated [11]. Afterwards, a radiative emission called phosphorescence happens, as it has longer wavelengths and longer lifetime than the fluorescence.

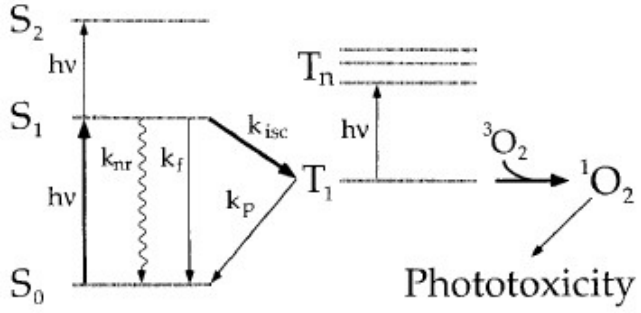

Figure 1 – Diagram of energy levels for the excitation by photons of a molecule. S_0, S_1 and S_2 represent the singlet electronic states of a molecule. T_1 and T_n represent the first and higher triplet electronic states of a molecule, respectively.

The transitions between states are depicted as vertical lines that illustrate the instantaneous nature of light absorption. The molecule can then undergo relaxation radiative or non-radiatively. k_{nr}, k_f, k_p and k_{isc} represent rate constants for non-radiatively decay, fluorescence decay, phosphorescence decay and intersystem crossing, respectively.

The energy losses between excitation and emission are observed for fluorescent molecules in solution. This effect is known as Stokes shift [12] that can be attributed to the rapid decay of fluorophores from higher states of energy to the lowest S_1 vibrational level. Fluorophores can also non-radiatively decay to higher S_0 vibrational levels. In order to arrive at ground-state it still undergoes further energy loss due to thermalization. Fluorophores can exhibit further Stokes shifts due to solvent effects, excited-state reactions, complex formation and energy transfer.

c. Porphyrins

To date, 400 compounds are known as photosensitizers and most of them are used in medicine, cosmetics and chemicals [8]. Single-molecule photosensitizers with low dark toxicity, adequate quantum yields (fluorescence, intersystem crossing and singlet oxygen formation), kinetic and thermodynamically stable with high stability are preferred over other fluorophores. First observation of tumor phototherapy (Haematoporphyrin derivative), first regulatory authorizations for clinical applications (Photofrin), one-pot synthesis, possibility for group substitution and interesting photochemical and photophysical properties make porphyrins and their derivatives one of the most significant group of molecules for use in PDT [13].

The parent compound for all porphyrins is porphin, a planar hetero-macrocycle with D_2h symmetry which consists of four pyrrolic moieties linked by their α-positions through methinic bridges [14]. The conjugated π-system contain 18 electrons along the shortest cyclic path and obeys the Hückel rule for aromatic systems. Two of the peripheral double bonds in the opposite pyrrolic rings are cross-conjugated and their presence is not needed for the aromaticity so the reduction of these bonds

maintains the aromaticity [15]. Porphyrins have intensive absorption bands in the visible range in particular, the optical spectrum shows a very strong absorption band at the 400-450nm region (Soret Band)) and in the 500-700nm bands (the Q bands) [16] (figure 2D). Porphyrins also show a remarkable thermal stability [9]

Porphyrins are substituted porphins with peripheral substituents which can be phenyl, pyridyl, 4-bromophenyl, etc. Other substituents can be positioned at the center of the macrocycles of these porphyrins (eg. Metalloporphyrins) [15].

In this study, two commercial available and water soluble porphyrins with different global charges were used: 5,10,15,20-(tetrakis)-(4-sulfonatophenyl) porphyrin (H_2TSPP^{-4}) and 5,10,15,20-(tetrakis)-(*N*-methyl-4-pyridinium-yl) porphyrin (TMPyP). H_2TSPP^{-4} is a tetra-anionic porphyrin that upon protonation of the nitrogen atoms (pKa≈4.8) within the macrocycle core forms H_4TSPP^{-2} with a zwitterionic character and high capacity of self-assembly (figure 2A) [17,18]. TMPyP is a tetra-cationic porphyrin (figure 2C) with high affinity with nucleic acids [19], preferential localization in tumor tissues, anti-HIV [20] and antibacterial activity [21] and reported use as active compound for singlet oxygen imaging of single cells [22] and for singlet oxygen photosensitization in skin fibroblasts [23].

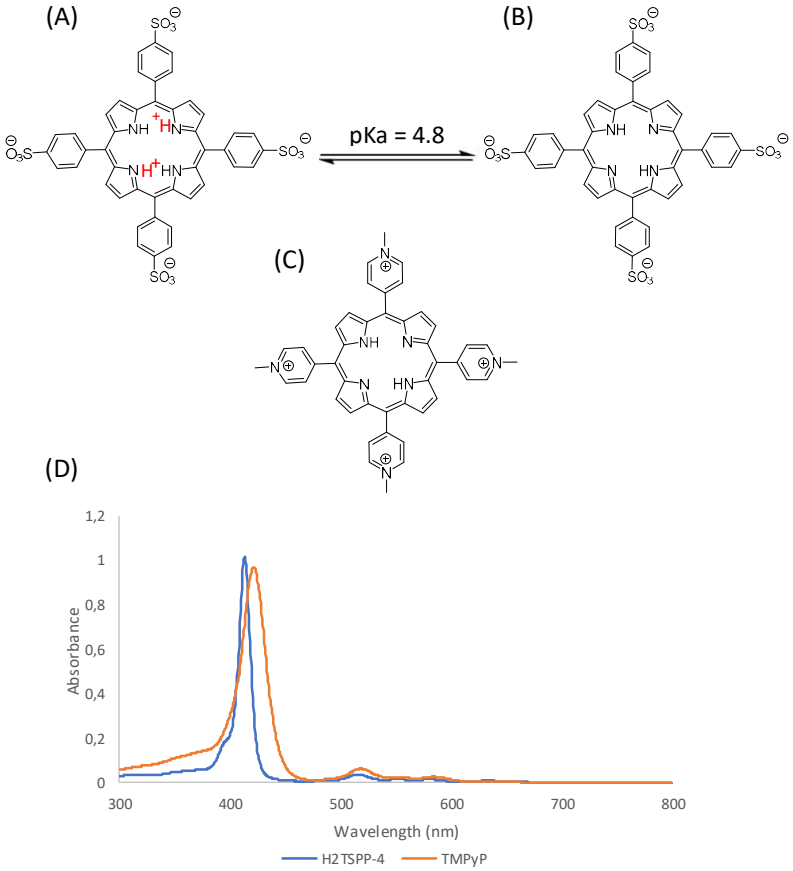

Figure 2 – (A,B) Acid-base equilibrium of H_2TSPP^{-4} in aqueous solution, (C) TMPyP molecular structure, and (D) UV-Vis absorption spectra of [H_2TSPP^{-4}] = 1.99x10^{-6} M and [TMPyP] = 3.90x10^{-6} M.

H_2TSPP^{-4} has four sulfonatophenyl groups as *meso*-subsitituents ($C_{44}H_{28}N_4NaO_{12}S_4^-$; Mr = 955.954 g/mol) [24]. In the equilibrium crystal structure of tetraphenylporphyrins, its *meso* phenyl

substituents are not co-planar with the macrocycles due to the intramolecular sterical hindrance between the hydrogen atoms in the *ortho*-positions of the phenyl rings and the adjacent hydrogen atoms at the porphin core [25]. This sterical hindrance leads to barriers to the rotation of the phenyl rings. The rotational motion of the phenyl rings is coupled to a saddle-shaped deformation of the porphyrin macrocycle by which the rotational barrier is reduced, during the transient co-planar orientation of phenyl rings and the macrocycles. The π-conjugation reaches a maximum, resulting in a further reduction of the rotational barrier [25]. At low pH values, H_4TSPP^{-2} can assemble into highly ordered aggregates which have already been observed [26,27] and are thought of as a result of the intermolecular electrostatic attractions between the positively charged core and the negatively charged periphery substituents of the monomer. Other factors are known to influence porphyrin aggregation in aqueous solution, such as concentration, temperature, ionic strength, metal ions and counterions. [17].

TMPyP has four pyridinium groups as *meso*-substituents ($C_{44}H_{42}N_8$; Mr = 682,858 g/mol). In this case, the environment has a great influence on its excited state properties [28]. In the presence of water, formation of hydrogen bonds between water molecules and the porphyrin core are observed, which increases the probability of energy dissipation through radiationless decay, reducing fluorescence quantum yield, and singlet and triplet excited-state lifetimes. TMPyP in organic solvents, however, demonstrates low sensibility to polarity and low ability to form hydrogen bonds.

d. Microcapsules

Several drug molecules cannot be formulated or administered by conventional techniques as they exhibit poor water solubility or have a short life-time in a complex environment such as the human body. There has been a rise in the need to develop systems that can carry and deliver precise quantities of such molecules to a specific target or tissue at a tailored release rate while protecting drug degradation by the body and the body from the side effects of the drug. In the last years, there has been a trend towards miniaturization that has challenged drug- delivery scientists to engineer novel systems. One of the relevant approaches was the development of Microcapsules, specifically polyelectrolyte microcapsules.

The microcapsules have begun to be designed and employed in various fields of application, such as pharmacy [29], food industry [30], agriculture [31], cosmetics [32], textile industry [33], printing [34], biosensor engineering [35], active coatings [36] and construction [37]. The interest and the demand of developing new custom microcapsules systems with different applications continues to rise and the scientific research is important to understand the fundamental properties for ground breaking innovation. The microcapsules formed by the Layer-by-Layer technique have attracted interest, particularly because of the ability to tailor their properties (size, composition, porosity, stability, surface functionality, colloidal stability). Therefore, these systems open the possibility to use a large variety of materials, including synthetic and natural polyelectrolytes, nanoparticles and biomacromolecules [38].

When devising and studying a polyelectrolyte microcapsule system, is important to have into account the core and polyelectrolyte characteristics and drug encapsulation, release and targeting profiles.

The core/template chosen for formation of the system was $CaCO_3$ obtained by mixing equal parts of $CaCl_2$ and Na_2CO_3. These microparticles with a size distribution of 4-6 μm and 30-50 nm porous sizes allow time-dependent permeability for different macromolecules. Its medium polydispersity can be controlled depending on experimental conditions: type of salts used and their concentration, pH, temperature and rate of mixing can contribute for uniform, homogenous and non-aggregated crystalline porous microcapsules [39]. Other characteristic of $CaCO_3$ microcapsules is their easy dissolution even after polyelectrolyte deposition [40].

Layer-by-Layer assembly (LbL) is an adsorption technique to prepare multilayered composite structures using the sequential adsorption of opposite charged materials. In polyelectrolytes the adsorption is self-limited as it is not possible to adsorb more polyelectrolyte once the surface it's fully charged. In the experimental part of the work the polymers used are poly(allylamine hydrochloride) (PAH) and poly(4-styrenesulfonic acid) (PSS) (figure 3) [41].

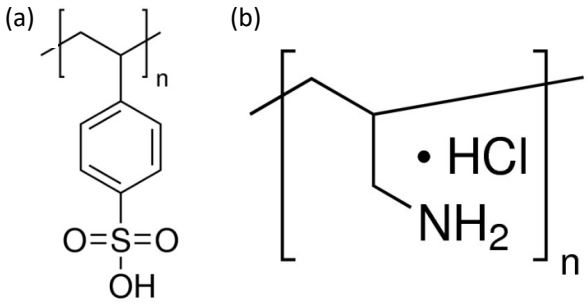

Figure 3 – Molecular structure of PSS (a) and PAH (b)

PAH is a cationic weak polyelectrolyte whose overall charge varies depending on environment pH. PSS is an anionic strong polyelectrolyte that maintains its charge over a wide range of pH values.

The self-assembly of PAH/PSS complex is driven by electrostatic interactions, polyelectrolyte conformation, as well as by entropy changes due to counterion release. Its formation is influenced by various physicochemical parameters like ionic strength, pH, temperature and solvent polarity [42]. Several parameters should be controlled such as the ratio of concentration of polyelectrolytes, the pH and ionic strength, in order to achieve an efficient LbL deposition.

In basic pH environments the multilayer film is bigger and less polydisperse than in acidic conditions This behavior is due to the modification of the fractional charge of PAH when the solution pH changes. The charges in a linear polyelectrolyte chain will repel each other, causing the chain to adopt a more expanded conformation. Polyelectrolyte complex formation, structure and morphology can be understood considering the ionic strength. For low concentrated salt solutions, ranging from 0.1M to 1.0M of NaCl is observed a decrease of the aggregation levels and an increase of the complex diameter

due to charge screening. For high concentrated salt solutions above 1.0M, it is observed secondary aggregation and an aggregated complex due to the excessive charge screening [42]. The salt concentration was selected as [NaCl] = 0.5M for suitable complex size and decreased polyelectrolyte aggregation.

The surface chemistry of the microcapsules dictates how they behave within a biological environment. This way, surface modification prevents the body from recognizing the capsules as foreign material and possibly deliver the capsules to particular locations within the body by targeting specific cell types. The recognition of a microcapsule as a foreign object by the body results in the destruction and excretion before cargo delivery. Various coatings like PEG [43] and lipids [44] have been applied to the outer layer of microcapsules to limit their interaction with biological environments: Cheng *et al.* [45] showed that nanoparticles coated with LbL films can be conjugated with branched PEG improving stability and lifetime in a physiological environment. Bio-functionalization of core-shell is possible for an increase in the target cell uptake directing to over-expressed targets. Integrins, folate receptors, or GD44 glycoproteins are examples of possible targets. Antibodies as biorecognition elements have already been used for successful targeting. Caruso *et al.* [46] demonstrated the increase in cell uptake in a line of colorectal cancer cells of LbL core-shells functionalized with the monoclonal antibody huA33.

There are two distinct profiles for releasing of therapeutic cargo once it has reached its target: instant (burst release) or slowly over an extended period (sustained release). Sustained release is desirable when the capsules should remain extracellular and so high doses can be dangerous or constant levels of drug are required [47]. The Burst release can be achieved by using an external stimulus to trigger degradation of the capsules. Different strategies have been proposed to engineer stimuli-responsive LbL microcapsules, with the aim of adjusting the permeability of the LbL and controlling the release of the cargo. The stimuli can be classified as chemical (pH, solvent, and electrochemistry) or physical (temperature, light, ultrasounds, magnetic fields and mechanical deformation) [48]. The change in pH from normal tissue (pH ~7.4) to cancerous tissue (pH~5) has motivated researchers to design pH-sensitive delivery vehicles for tumor cells. Luo *et al.* [49] prepared pH-responsive microcapsules with interaction between polyaldehyde dextran-graft-adamantane (PAD-g-AD) and carboxymethyl dextran-graft-β-cyclodextran (CMD-g-β-CD). The pH-responsiveness was due to acid-sensitive hydrazine bonds in the PAD-g-AD. DOX (Doxorubicin) was loaded into the wall of the microcapsules by conjugation with AD through hydrazones. At the tumor sites, the hydrazone bonds were disrupted and AD groups were removed, leading to the destruction of the microcapsules and the release of DOX.

Drug Release can also be triggered by light activation, such as near-infrared (NIR) light. Wu *et al.* [50]. described a proof-of-concept application of a multilayer vehicle for drug delivery and NIR light-controlled release induced by the film-loaded AuNPs. They first coated a porous template with poly(L-lysine)/bovine serum albumin (PLL/BSA) films and then added a temperature-sensitive gelatin hydrogel that was loaded with DOX and AuNPs. After the template dissolution, the drug delivery system was ready and DOX could be released into the surrounding medium via light-induced melting of the gelatin hydrogel.

The Burst release method can also be triggered via the intracellular uptake process itself, since in this case the capsule can be cross-linked by disulfide bridges where although it can be retained in the bloodstream, in the oxidizing environment of the cell, the disulfide linkages would be disrupted [51].

CHAPTER 2

Experimental Techniques

a. UV-Vis Absorbance

One of the equipment's used was the absorption spectrophotometer in the (UV-Vis) range, in which the efficiency of light absorption at a wavelength λ by an absorbing medium is characterized by the absorbance A (λ) or the transmittance T (λ) defined as [52]:

$$A\ (\lambda) = \log \frac{I_\lambda^0}{I_\lambda} \quad (1)$$

$$T\ (\lambda) = \frac{I_\lambda}{I_\lambda^0} \quad (2)$$

Following the Beer-Lambert Law, the equation (1) can be described as:

$$A\ (\lambda) = \varepsilon(\lambda) l c \quad (3)$$

Where ε(λ) is the molar absorption coefficient (expressed in $Lmol^{-1}cm^{-1}$), c is the concentration (mol L^{-1}) of absorbing species and l is the absorption path length (cm).

Derivation of the Beer-Lambert Law from considerations at a molecular scale is more interesting than the classical derivation (which states that the fraction of light absorbed by a thin layer of the solution is proportional to the number of absorbing molecules). Each molecule has an associated photon-capture area, called the molecular absorption cross-section σ, which depends on the wavelength. A thin layer of thickness dl contains dN molecules. dN is given by (4):

$$dN = Na \cdot c \cdot S \cdot dl \quad (4)$$

Where S is the cross section of the incident beam and Na is the Avogadro's number. The total absorption cross-section of the thin layer is the sum of all molecular cross-sections, dN. The probability of photon capture is σdN=S and is simply equal to the fraction of light (-dI/I) absorbed (5):

$$-\frac{dI}{I} = \frac{\sigma dN}{S} = Na \cdot \sigma \cdot c \cdot dl \quad (5)$$

$$ln \frac{I_0}{I} = Na \cdot \sigma \cdot c \cdot l \quad (6)$$

$$log \frac{I_0}{I} = \frac{1}{2.303} Na\sigma cl \quad (7)$$

$$\sigma = \frac{2.303\varepsilon}{Na} = 3.825 \times 10^{-19}\varepsilon \quad (8)$$

For the practical use of the Beer-Lambert law, in general, the sample is a solution placed in a cuvette. The absorbance is characteristic of the absorbing species. Therefore, it is important to note that in the Beer-Lambert law, I_0 is the intensity of the beam entering the solution but not is the incident beam

I_i on the cuvette, and I is the intensity of the beam leaving the solution but not the beam I_s leaving the cuvette. In fact, there are some reflections and absorptions (in a less extent). Moreover, the solvent is assumed to have no contribution, but it may also be partially responsible for a decrease in intensity because of scattering and possible absorption.

The contributions of the cuvette walls and the solvent can be taken in account, using the equations in figure 4. Using double-beam spectrometers, it automatically records the true absorbance of the sample, thanks to a double compartment containing two cuvettes, one filled with the solution and one filled with the solvent.

When starting a measurement, the baseline of the instrument is recorded and stored. [52].

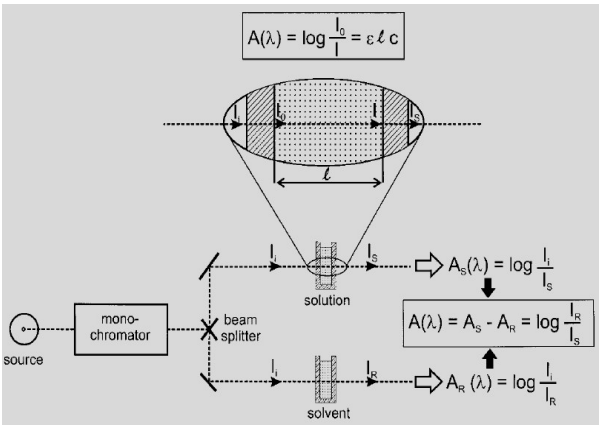

Figure 4 – Absorbance measurements in a double-beam spectrophotometer [53].

b. Zeta Potential

Another measure done was the zeta-potential which is a key parameter to control surface charge of particles.

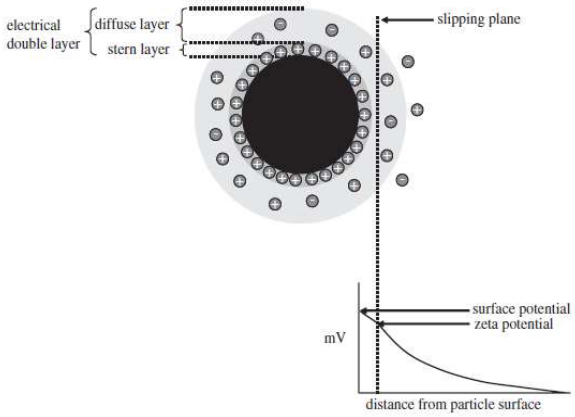

Figure 5 – Zeta-Potential, measured at the boundary of the surface. [54]

Most colloidal dispersions in aqueous media carry an electric charge and the development of this charge at the particle surface affects the distribution of ions in the surrounding interface region (figure 5,6).

An increase in the concentration of counter ions close to the surface results in the formation of an electrical double layer. The liquid layer surrounding the particle can be divided in two parts. The inner region is called Stern Layer where the ions are strongly bound and an outer (diffuse) region where they are less firmly associated. When the particle moves, the boundary moves with it. The potential at this boundary is called the zeta potential [53].

The zeta potential of the colloidal dispersion can be measure using the technique of micro-electrophoresis [54]. In this technique, a voltage is applied across two electrodes at either end of the cell containing the particle dispersion. Charged particles are attracted to the oppositely charged electrode and their velocity is measured and expressed as their electrophoretic mobility. Light scattering is one of the most commonly used techniques for determining the electrophoretic mobility of particles. Laser Doppler electrophoresis measures the frequency shifts in the scattered light that arise owing to the movement of particles in an applied electric field (9).

$$\Delta f = \frac{2v\sin(\frac{\theta}{2})}{\lambda} \qquad (9)$$

Where v is the particle velocity, λ is the wavelength of the incident light and θ is the scattering angle. The measured electrophoretic mobility (U_E) is converted into zeta potential (ζ) through Henry's equation (10).

$$U_E = \frac{2\varepsilon\zeta F(ka)}{3\eta} \qquad (10)$$

Where ε is the dielectric constant of the dispersant, F(ka) is the Henry function and η is the viscosity. This equation only applies for isolated particles of zeta potential less than 25mV. In large particles, when F(ka)=1,5, the Henrys equation transforms in the known Smoluchowski equation [55], and applies when ka is large and the double layer is thin by comparison with the particle radius.

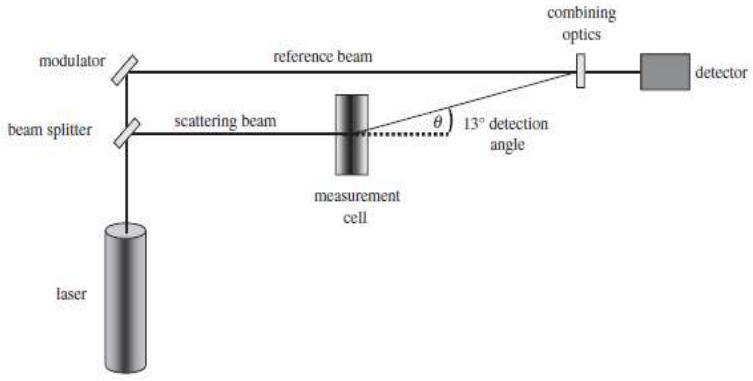

Figure 6 - Laser Doppler electrophoresis instrument. [54]

c. Fluorescence Emission and Light Excitation

To measure the fluorescence emission or the excitation spectra of a molecule is necessary to use a spectrofluorometer. The device has a light source, generally a high - pressure xenon arc lamp, which offers the advantage of continuous emission from ~250 nm to the near infrared. It has a monochromator which is used to select the excitation wavelength.

The fluorescence is collected at right angle with respect to the incident beam and detected through a monochromator by a photomultiplier. Automatic scanning of wavelengths is achieved by the motorized monochromators, which are controlled by the electronic devices and the computer (figure 7).

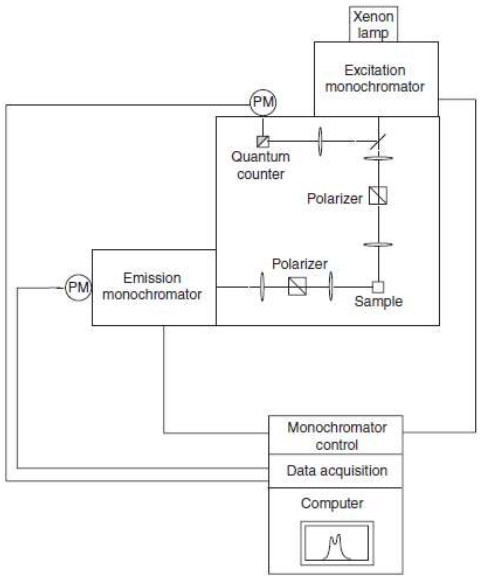

Figure 7 –Conventional spectrofluorometer [52].

The optical module contains various parts: a sample holder, shutters, polarizers and a beam splitter consisting of a quartz plate reflecting a few percentage of the exciting light toward a quantum counter or a photodiode [52]. A reference channel has two advantages: it compensates for the time fluctuations of the lamp intensity via a ratiometric measurement and it permits a correction of excitation spectra.

Emission and excitation spectra are defined using the following expression for the measured fluorescence intensity (11):

$$I_F\ (\lambda_E, \lambda_F\ )\ =\ kF(\lambda_F\ )I_0\ (\lambda E\ )\{1-\ exp[-2.3\varepsilon(\lambda_E\ )lc\ ]\}\ (11)$$

Where λ_E is the excitation wavelength, λ_F is the wavelength at which the fluorescence is observed, I_0 is the intensity of the incident beam on the sample, ε (λ_E) is the molar absorption coefficient at the excitation wavelength, l is the optical path in the sample, *c* is the molar concentration, and A (λ_E) is the absorbance at the excitation wavelength, F (λ_F) is the variation in fluorescence intensity per unit wavelength. k is an instrumental factor that depends on many parameters: geometry of observation (solid angle through which the light is collected), monochromators transmission efficiency, width of the

monochromator slits, high voltage of the photomultiplier and gain of the electronic devices. Therefore, the numerical value of the measured fluorescence intensity has no meaning and the fluorescence spectrum is usually plotted in arbitrary units.

The emission spectrum corresponds to the variations of I_F as a function of λ_F, the excitation wavelength λ_E being fixed, whereas the excitation spectrum reflects the variations of I_F as a function of λ_E, the observation wavelength λ_F being fixed.

d. Fluorescence Lifetime Imaging (FLIM)

Fluorescence Lifetime Imaging (FLIM) produces an image based on the differences in the excited state decay rate from a fluorescent sample. FLIM is a fluorescence imaging technique where the contrast is based on the lifetime of individual fluorophores rather than their emission spectra. The fluorescence lifetime is defined as the average time that a molecule remains in an excited state prior to returning to the ground state by emitting a photon (figure 8).

As the fluorescence lifetime does not depend on concentration, absorption by the sample, sample thickness, photo-bleaching and/or excitation intensity are more robust than intensity based methods [56]. The excited-state lifetime of a fluorophore is sensitive to its microenvironment.

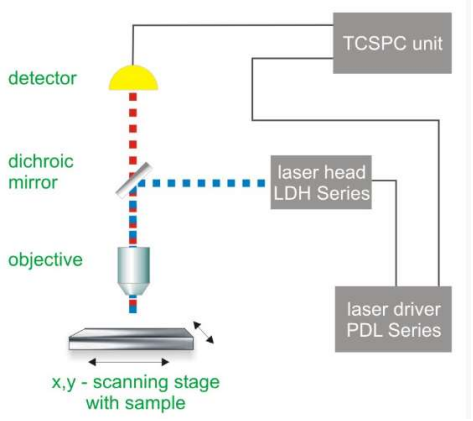

Figure 8 - Generalized setup of a fluorescence lifetime imaging microscope [56].

Therefore, imaging of the lifetime provides complementary information on local physical parameters and chemical parameters in addition from the steady-state characteristics. Some applications of FLIM that have been reported are calcium (or other chemical) imaging; membrane fluidity, transport and fusion; imaging using RET (resonance energy transfer) for quantifying the distance between two species labeled with different fluorophores; DNA sequencing; Clinical imaging. FLIM has been developed using either time-domain or frequency-domain methods. In this study, it was used the time-domain FLIM.

In principle, lifetime imaging is possible by combination of the single-photon timing technique with scanning techniques. However, the long measurement time required for collecting photons at each point is problematic. Alternatively, a gated microchannel plate (MCP) image intensifier can be used in

conjunction with a slow-scan cooled CCD camera for digital recording. Laser picosecond pulses are used to illuminate the entire field of view via an optical fiber and a lens of large numerical aperture. At time t_d after excitation by a light pulse, a sampling gate pulse (duration Δt) is applied to the photocathode of the image intensifier. Fluorescence can thus be detected at various delay times (multigate detection). For a single exponential decay of the form α exp (-t/τ), two delay times t_1 and t_2 are sufficient (figure 9).

The corresponding fluorescence signals D_1 and D_2 given by:

$$D_1 = \int_{t_1}^{t_1+\Delta t} \alpha \exp(-\frac{t}{\tau})\ dt \qquad (11)$$

$$D_2 = \int_{t_2}^{t_2+\Delta t} \alpha \exp(-\frac{t}{\tau})\ dt \qquad (12)$$

By this procedure, which requires calculation from only four parameters (D_1; D_2; t_1 and t_2), lifetime images can be obtained. Time-resolved images can be accumulated on the CCD chip by repeated pulse excitation. The images are then read out to a computer [52].

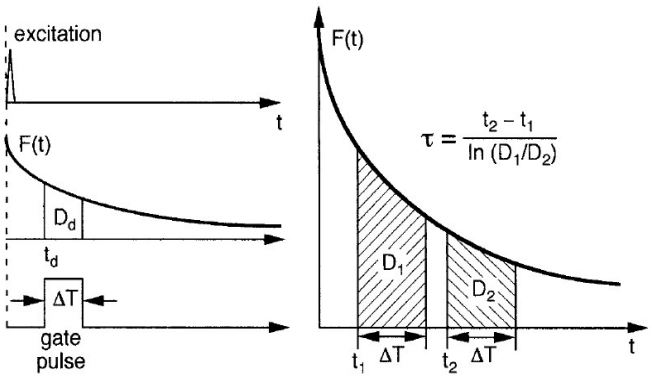

Figure 9 - Principle of lifetime measurement by the gated image intensifier [52].

e. Transmission Electron Microscopy (TEM)

A transmission electron microscope (TEM) is an instrument that is used to directly visualize small or thin samples using electrons rather than photons as an illumination source. Typical components of a typical TEM are an electron gun to illuminate the specimen, condenser lenses to focus the electrons, an objective lens to form the image, intermediate and projector lenses to magnify the image, and either a fluorescent screen or charge-coupled device (CCD) camera (or film) to observe or record the image. Ernst Ruska in 1933 showed that electrons, with their much shorter wavelengths than light, could produce higher resolution images from a microscope.

The most common electron gun in these instruments is called a thermionic gun. Thermionic guns work by applying a current to the filament to create a hot cathode. As current is applied to the filament, the filament becomes hotter. As the thermal barrier (work function) keeping the electrons bound

to the filament is exceeded, electrons are ejected into the column by a process called thermionic emission (figure 10).

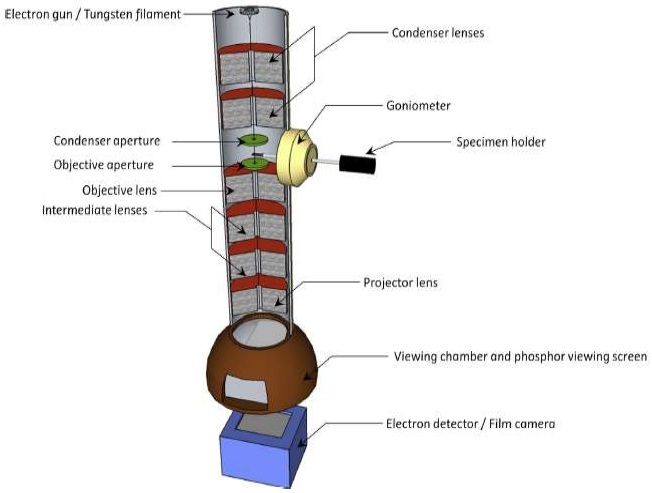

Figure 10 - Design and layout of a generic transmission electron microscope [57].

The ejected electrons are then accelerated toward the anode and focused through an electrostatic lens. As the electrons accelerate through the Wehnelt and pass the anode, they encounter the condenser lenses (two or three), which focus the beam of electrons and pass them through the condenser aperture to evenly illuminate the thin sample. Once the electrons exit the condenser aperture, they evenly illuminate the specimen.

The interaction between the specimen and the electron beam produces different types of radiation: Direct beam; Coherent beam; Incoherent Beam; Elastic Beam and Inelastic Beam. When the beam impinges on and passes through the specimen, a significant portion fails to interact with it at all and is unaffected by the specimen. This is called the direct beam.

A coherent beam is one in which all of the electrons are in phase with each other and have the same wavelength, energy, and speed. In an incoherent beam, the electrons have different wavelengths, different energies, and travel at different speeds in different directions. After the beam passes through the specimen, elastic or inealastical electrons are detected.

Elastic electrons retain their energy and speed with a negligible amount of energy loss after passing through the specimen. Inelastically scattered electrons have lost a significant portion of their energy as a result of interaction with the specimen.

The direct and scattered beam passes through the objective lens. The objective aperture serves two important roles. Its first role is to filter out the electrons scattered to high angles. Its second role is to increase the image contrast reducing the charge that builds up as a result of exposure to the electron beam.

The escape of electrons from the specimen builds a net positive charge upon the specimen surface that deforms the specimen and acts as an imperfect lens that distorts the image. When the objective aperture is inserted, the scattered beam coming from the specimen affects the aperture and produces back-scattered electrons that travel back to the specimen.

Since these electrons have less energy than the incident beam, they affect the specimen and remain, tending to neutralize the positive charge accumulating in the specimen. Without the aperture, nonconductive biological specimens like thin sections from resin-embedded tissue prepared by ultramicrotomy can overcharge, melt, and break before they can be imaged because of the charge.

The intermediate lenses and the projector lens are used to set the magnification of the image and project it either onto a fluorescent screen or onto a CCD camera or film for recording [57].

CHAPTER 3

Experimental Section

a. Materials

Poly(styrenesulfonate), PSS (MW ~ 75000, 18% wt.%), poly(allylamine hydrochloride), PAH (MW ~ 15000), H_2TSPP^{-4} (ε_{413} = 5.1x10^5 M^{-1}cm^{-1}) and TMPyP (ε_{422} =2.49x10^5 M^{-1} cm^{-1}) were obtained from Sigma-Aldrich. Diammonium ethylenediaminetetraacetate monohydrate, EDTA (MW ~326) was obtained from TCI. Sodium hydroxide (NaOH) and hydrochloric acid (HCl) were used to control pH and were purchased from Sigma-Aldrich. All reagents were used as obtained. Polyelectrolyte solutions (3 mg/mL, 0.5 M NaCl) were prepared in bi-distilled water and adjusting pH at 6.5 (NaOH) or pH 3.0 (HCl). H_2TSPP^{-4}, TMPyP solution (3x10^{-4}M) and EDTA were prepared in bi-distilled water.

Preparation of $CaCO_3$. $CaCO_3$ used for the polyelectrolyte core was obtained by adding equal volumes of $CaCl_2$ (0.1M) and Na_2CO_3 (0.1M) and mixed for one minute under intense stirring and let to rest for 5 minutes. $CaCO_3$ microparticles were recovered after supernatant removal followed by three washing/centrifugation cycles.

Preparation of Polyelectrolyte Microcapsules. The polyelectrolyte microcapsules were prepared by dispersing the $CaCO_3$ template in an aqueous PAH (3mg/ml, 0.5M NaCl) solution. After stirring for 30 minutes and centrifugation (6000 rpm, 10 minutes), the particles are recovered and the supernatant removed. After three washing/centrifugation cycles to remove the excess PAH, the particles are resuspended in an aqueous PSS (3mg/ml, 0.5 NaCl) solution. This layer-by-layer deposition technique of opposite charged polyelectrolytes was repeated until four or five polyelectrolyte layers were adsorbed.

Porphyrin Adsorption onto Polyelectrolyte Microcapsules. H_2TSPP^- or H_4TSPP^{-24} and TMPyP were adsorbed onto polyelectrolyte microcapsules with PAH and PSS as the last layer, respectively. Polyelectrolyte microcapsules resuspended in water were added to a porphyrin solution (3μM, pH 6.5 or pH 3.0) and mixed for one hour. After centrifugation the supernatant is removed and stored and the functionalized microcapsules are washed three times with distilled water (pH 6.5 or pH 3.0).

Polyelectrolyte Microcapsules Porphyrin Release. In a quartz cuvette porphyrin dopped polyelectrolyte microcapsules are added to a release solution. A gastric solution, was prepared by dissolving 0,2% (w/v) NaCl in water and adjusting pH 2.0 (HCl) and an intestinal solution was prepared by dissolving 0,68% (w/v) KH_2PO_4 in water with and adjusting pH = 7,2 (NaOH) [58]. The supernatant fluorescence emission is then measured, under stirring, over time.

Preparation of Hollow Polyelectrolyte Microcapsules. Hollow polyelectrolyte microcapsules were obtained by suspending microcapsules in EDTA (10 mL, 0.1 M) and stirring for 30 min at room temperature. This process was repeated twice. The prepared hollow polyelectrolyte microcapsules were washed three times with distilled water before further use.

Formation of J-aggregates on Polyelectrolyte Microcapsules. The polyelectrolyte microcapsules were left overnight at room temperature in an aqueous solution of H_4TSPP^{-2} at pH =3.0 without stirring. Afterwards, the supernatant is removed and the PECs are washed with distilled water at pH 3.0.

b. Methods

A Jasco V-560 and a Hitachi (U-2000) spectrophotometers were used in UV–vis absorption measurements. Corrected fluorescence measurements were recorded with a SPEX Fluorolog spectrophotometer (Horiba Jobin Yvon).

FLIM measurements were performed with a time-resolved confocal microscope (MicroTime 200, PicoQuant GmbH). The excitation at 483 nm/639 nm was carried out by a pulsed diode laser at a repetition rate of 10/20 MHz. The fluorescence lifetime was detected with a single-photon counting avalanche diode (SPAD) (PerkinElmer) whose signal is processed by TimeHarp 200 TC-SPC PCboard (PicoQuant) working in the time-tagged time resolved (TTTR) operation mode. For point-by-point measurements, fluorescence decays of more than thirty-pixel points were collected from random points chosen within microcapsules.

The pH was measured at 24.0◦C with a Denver Instrument Model 215 pH sensor and the adjustment to the desired pH values accomplished by the addition of HCl or NaOH.

The zeta potential values were measured in a Doppler electrophoretic light scattering analyzer, Zetasizer Nano ZS from Malvern Instruments Ltd.

Transmission Electron Microscopy (TEM) images were obtained by a Hitachi 8100 transmission electron microscope operating at 200 kV with an energy dispersive X-ray spectrometer (EDS).

The light-mediated release was done using with a mounted High-Power LED (595L3) from THORLABS with a nominal wavelength of 595nm allowing to achieve an irradiance of 0.5mW/cm2.

CHAPTER 4

Porphyrin Interaction with Polyelectrolyte Microcapsules

The optical properties and amount of the fluorophore adsorbed onto polyelectrolyte microcapsules are important conditions to infer the system PDT efficiency. Three different polyelectrolyte microcapsules systems were designed and prepared. These systems have four or five layers of positive and negative polyelectrolytes and a porphyrin is adsorbed in the last one (figure 11). $CaCO_3$(PAH/PSS)$_2$PAH H_2TSPP^{-4}, $CaCO_3$(PAH/PSS)$_2$ H_2TSPP^{-4} and $CaCO_3$(PAH/PSS)$_2$ TMPyP were obtained using layer-by-layer methodologies.

The first part of this chapter is dedicated to the optimization of the experimental procedure in order to achieve the best pH conditions for layer-by-layer assembly and porphyrin loading, followed by a detailed study on the optical properties (UV-Vis absorption and steady state emission) and FLIM of the optimized systems. In the second part of the chapter, the encapsulation efficiency and release kinetic profiles were determined and compared.

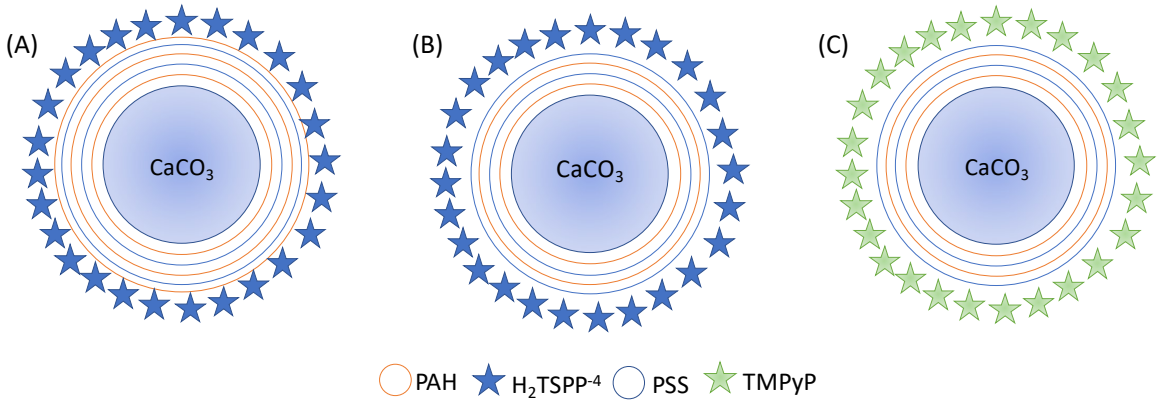

Figure 11 – Polyelectrolyte microcapsules studied. (A) $CaCO_3$(PAH/PSS)$_2$PAH H_2TSPP^{-4}, (B) $CaCO_3$(PAH/PSS)$_2$ H_2TSPP^{-4} and (C) $CaCO_3$(PAH/PSS)$_2$ TMPyP.

a. H_2TSPP^{-4} Interaction – UV-Vis Absorption and Emission studies

To study the interactions of H_2TSPP^{-4} with polyelectrolyte microcapsules, we started by adsorbing a H_2TSPP^{-4}solution at pH 6.5 onto pre-formed $CaCO_3$ (PAH /PSS)$_2$ PAH structures. After the adsorption and washing procedures the UV-Vis absorbance spectrum was acquired and analyzed (figure 12). It was observed a spectrum composed by two main bands in Soret region (413 nm and 430 nm) and four bands in the Q-region (500-700 nm) one at 413 nm corresponding to the Soret band of H_2TSPP^{-4} and another red shifted band at 430 nm.

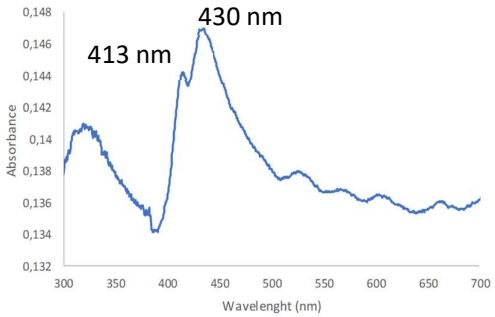

Figure 12 – UV-Vis spectrum of $CaCO_3$(PAH/PSS)$_2$PAH H_2TSPP^{-4} (pH 6.5).

In a first glance to justify the presence of these two bands, we started by studying the interaction of H_2TSPP^{-4} which each one of polyelectrolytes (PAH and PSS) in solution by absorption and emission spectroscopy (figure 13 and table 1).

Table 2 – Maxima absorption (λ_A^{max}) and emission (λ_{em}^{max}) (for H_2TSPP^{-4} in water, PAH and PSS polyelectrolyte solutions.

	λ_A^{max} (nm)	λ_{em}^{max} (nm)
H_20 (pH=7) [(a)]	413	650;708
PAH [(a)]	400	650;708
PSS [(b)]	420	650;718

(a) $\lambda_{exc} = 413$ nm (b) $\lambda_{exc} = 420$ nm

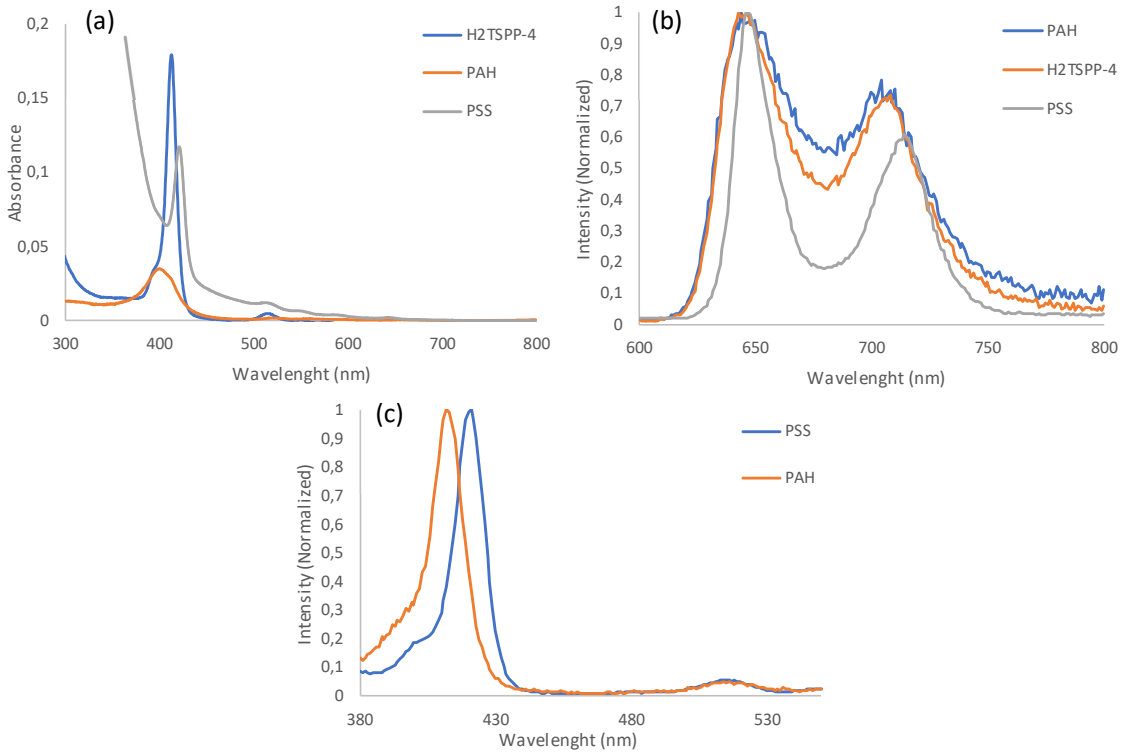

Figure 13 – UV-Vis absorption (a), fluorescence (λ_{exc}*H2TSPP-4, PAH* = *413 nm;* λ_{excPSS} = 420 nm) (b) and excitation spectra (λ = 650 nm) (c) of H_2TSPP^{-4} ($3.9x10^{-7}$M) in water and polyelectrolyte solutions

The interaction of H_2TSPP^{-4} with PAH is electrostatically favored as H_2TSPP^{-4} and PAH have opposite charges. This interaction is verified by a broadening of the Soret band in the H_2TSPP^{-4} absorption spectrum and a hypsochromic shift of the maximum wavelength from 413 nm to 400 nm, characteristic of H-aggregates formation.

It was chosen an excitation wavelength of 400 nm to obtain the emission spectrum of H_2TSPP^{-4} in a PAH solution. Nevertheless, the emission spectrum has the same form and both two maximum

wavelengths for 650nm and 708nm as H_2TSPP^{-4} in aqueous solution at pH=7 (figure 13 b). Also, the excitation spectra obtained at 650 nm (Figure 13 c) overlaps in each point its absorption spectra of H_2TSPP^{-4} in water. Therefore, the fluorescence observed should be a result of the remaining monomeric H_2TSPP^{-4}.

The H_2TSPP^{-4} interaction with PSS is not electrostatically favored as both porphyrin and polyelectrolyte have the same charge. Nevertheless, the interaction of H_2TSPP^{-4} and PSS promote a bathochromic shift of the Soret band from 413 nm to 420 nm. When using 420nm as an excitation wavelength, the maximum emission wavelength for the solution of H_2TSPP^{-4} and PSS is 650nm and 718nm. The second maximum is the only with a visible change (~10nm) which implies a modification of the vibrionic levels of H_2TSPP^{-4} as the overlap of both bands is also reduced when compared with the free-base H_2TSPP^{-4} at pH=7.

By comparison of the spectra of H_2TSPP^{-4} in PAH solution with the ones observed previously for microcapsules resuspended in water at pH 6.5 (figure 12), it is possible to infer that the interaction of PAH as the microcapsules external layer, does not induce the formation of H aggregates as it occurs in solution. Two main reasons may be in the origin of this observation: a lower concentration of PAH adsorbed or a preferential location of H_2TSPP^{-4} in more hydrophilic environments such as interstitial water as revealed by the presence of the absorption band at 413 nm and the typical emission bands of H_2TSPP^{-4} in water. Another interesting point is the changes observed in the absorption spectra of H_2TSPP^{-4} due to the presence of PSS. Although the wavelength maxima of the unknown band at 430 nm in polyelectrolyte microcapsules is 10 nm red shifted when compared to the one Soret band of H_2TSPP^{-4} in PSS solution the possibility that the two are due to the same type of interaction should not be disregarded, since the differences accounted for may be related with adsorption.

In order to best understand the porphyrin interaction with each one of the polyelectrolyte constituents in PECs, the effect of the pH of the last layer was studied. PECs were washed with water at pH 3.8, 4, 5, 6.5 and 8 and the zeta potential was measured (figure 14). A total reversal of zeta potential was observed for pH 3.8 and 4.

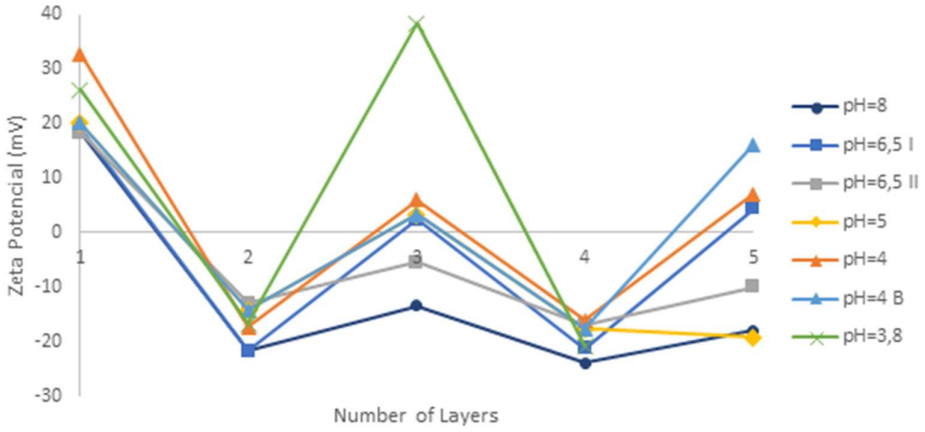

Figure 14 – Effect of the pH of the washing solution on the zeta potential of the polyelectrolyte microcapsule. It was done two different measurements for pH =6.0, 5.0 and 4.0. For 4.0 B, only the last layer was washed with pH=4.0 between the rest of them washed with pH=5.0.

After optimizing the experimental pH for the total reversal of the surface zeta potential, two different experiments were designed. The conditions used were $CaCO_3(PAH/PSS)_2PAH$ with a washing pH of 4.0 adsorbed with a H_2TSPP^{-4} solution with pH 6.5 and $CaCO_3(PAH/PSS)_2$ with a washing pH of 6.5 adsorbed with a H_2TSPP^{-4} solution with pH 8.0 (figure 15).

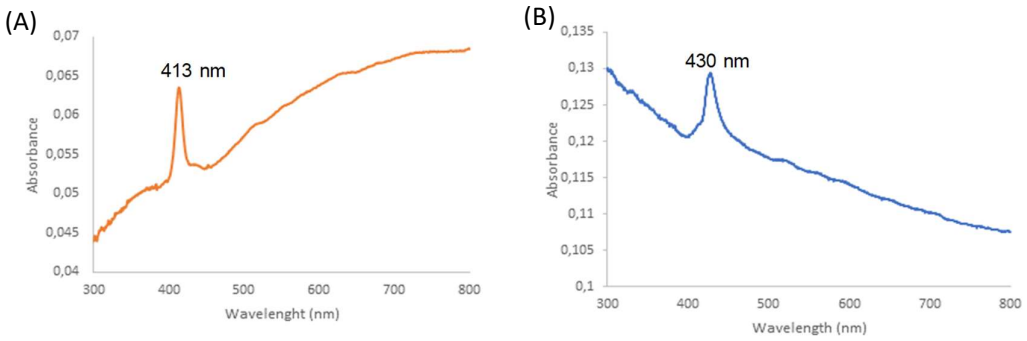

Figure 15 – UV-Vis spectra of (A) $CaCO_3(PAH/PSS)_2PAH$ H_2TSPP^{-4} and (B) $CaCO_3(PAH/PSS)_2$ H_2TSPP^{-4} systems in water.

It is interesting to note that the nature of the polyelectrolyte last layer as well as the surface charge has a direct outcome on H_2TSPP^{-4} interactions within polyelectrolyte microcapsules. For $CaCO_3(PAH/PSS)_2PAH$ microstructures with a positive last layer, only one band in the Soret region of the absorption spectra with a maximum wavelength at 413 nm was detected. In contrast, when H_2TSPP^{-4} was adsorbed onto polyelectrolyte microcapsules $CaCO_3(PAH/PSS)_2$ with a negative last layer, the only absorption band observed in the absorption spectra has its maximum at 430 nm. Nevertheless, it was possible to design two systems where the appearance of only one specific H_2TSPP^{-4} form is obtained.

In the first system the low pH should increase the protonation of PAH and increase water polyelectrolyte microcapsules content, leading to a higher adsorption of H_2TSPP^{-4} in water rich environments, as reflected by the presence of the absorption band at 413 nm. In the second system, the lower protonation of PAH and the last layer PSS increased the hydrophobicity and electrostatic repulsion of the system. In this case the adsorption of H_2TSPP^{-4} near PSS, probably mediated by counterions, or its location in more hydrophobic environments should be preferred. Bédard *et al.* reported a red shift on the Soret band of H_2TSPP^{-4} sandwiched between PAH and PSS layers to 424 nm. [47].

The difference observed in spectra baseline is related with the dispersion of light due to polyelectrolyte microcapsules Brownian motion. In the $CaCO_3(PAH/PSS)_2PAH$ H_2TSPP^{-4} system, the microcapsules have a tendency to deposit in the cuvette. In the $CaCO_3(PAH/PSS)_2$ H_2TSPP^{-4} system, the microcapsules tend to suspend in solution.

To proceed the study of the differences of H_2TSPP^{-4} form in polyelectrolyte microcapsules, it was examined the emission spectrum of both systems present in figure 15. The excitation and deexcitation of a fluorescent molecule is related to the electronic transition induced by photon absorption

that consists of the passage of electrons from a lower electronic state, ground state, to a state of higher energy and return back to the ground state [52].

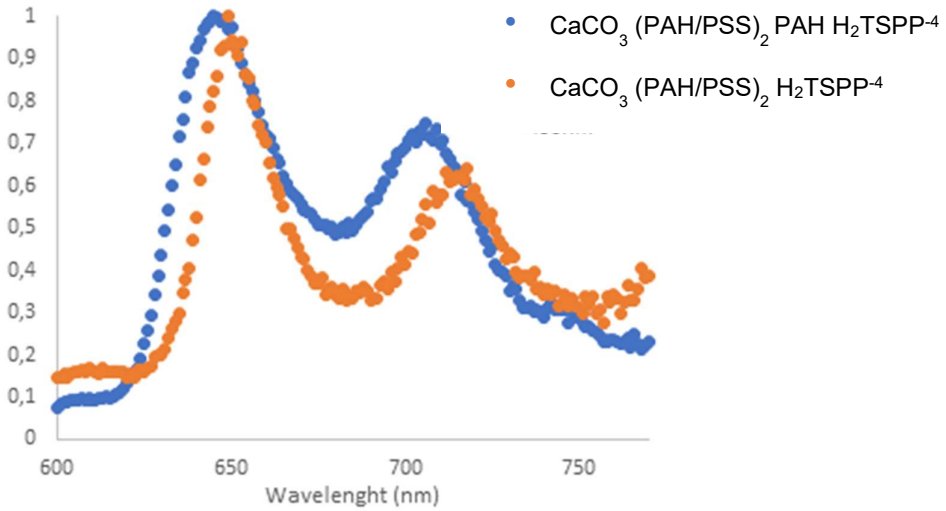

Figure 16 - Normalized Emission Spectra of H_2TSPP^{-4} adsorbed on polyelectrolyte microcapsules for easier comparison.

The differences between both systems are a slight shift to the higher wavelengths (~4-14nm) accompanied by an overall decrease of fluorescence emission probably due to lower porphyrin concentrations (see next section). Interestingly the emission spectra of $CaCO_3(PAH/PSS)_2PAH$ H_2TSPP^{-4} and the emission spectra of $CaCO_3(PAH/PSS)_2$ H_2TSPP^{-4} are quite comparable to the ones obtained for H_2TSPP^{-4} in water and in PSS solutions, respectively, in accordance with the previous results obtained by absorption spectroscopy.

The excitation spectra of both systems were also measured and analyzed. The excitation spectrum is an important measure as it provides useful information regarding the presence of different fluorescent species or when a sole species is present in different forms in the ground state energy level. In the presence of a single type of molecules in the ground state the corrected excitation spectrum is identical in shape with the absorption spectrum of that same molecule. If that is not verified is possible to conclude that the molecules are present in different forms in the solution as in form of aggregates, complexes or tautomeric forms.

Using the information of the emission spectra of both systems in figure 16, it was selected the emission wavelength for which the excitation of the system was monitored. For the polyelectrolyte microcapsule system $CaCO_3(PAH/PSS)_2PAH$ H_2TSPP^{-4}, the emission wavelengths selected for the excitation spectrum were 650 nm and 718nm (figure 16).

The excitation spectra obtained allows to confirm that the emission peaks of $CaCO_3(PAH/PSS)_2PAH$ H_2TSPP^{-4} match with the absorbance spectrum of the same system. It is then possible to confirm that the emission spectra obtained only regards monomeric H_2TSPP^{-4} in water (figure 17).

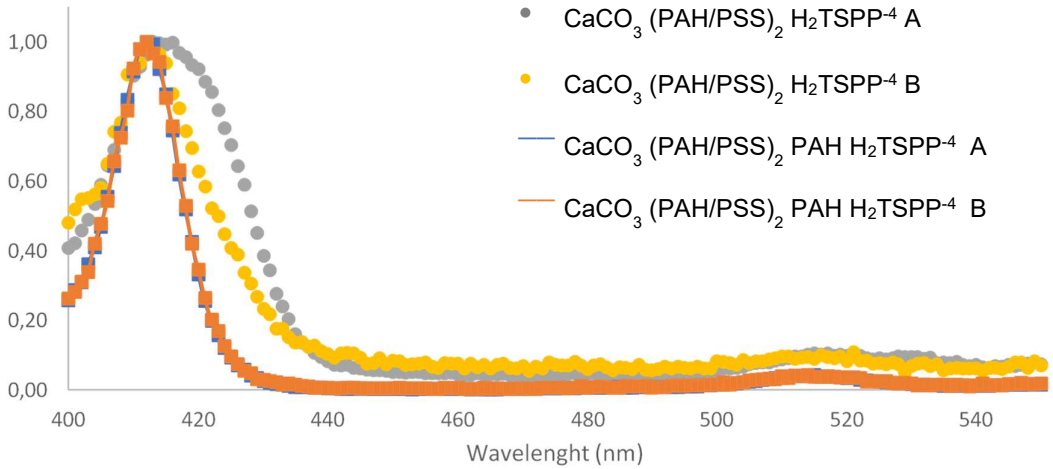

Figure 17– Excitation Spectra normalized of H_2TSPP^{-4} on both polyelectrolyte microcapsules systems. A- λ_{em}=650 nm; B- λ_{em}=718nm.

To conclude, the study done with H_2TSPP^{-4} in sole interaction with the polyelectrolytes did not give a straight answer regarding the shift of Soret band maximum of the absorbance spectrum to 430 nm. In the system $CaCO_3(PAH/PSS)_2$, H_2TSPP^{-4} is electrostatically repulsed as it has the same charge of PSS polyelectrolyte and the deprotonation of PAH caused by the increase of the pH value, decreased the volume of water present inside the microcapsule and the mobility of charged counterions [59]. H_2TSPP^{-4} absorbance maximum at 430 nm should be consequence of an arrangement of H_2TSPP^{-4} monomers, that are spread in certain hydrophobic domains near PSS polyelectrolyte.

TMPyP Interaction – UV-Vis Absorption and Emission studies

Similarly to H_2TSPP^{-4} the adsorption of TMPyP onto polyelectrolyte microcapsules $CaCO_3(PAHPSS)_2$ was also followed by UV/Vis absorption and Fluorescence Spectroscopy.

The TMPyP UV-Vis spectrum changes whether it is present in solution and when it is adsorbed in polyelectrolyte microcapsules (figure 18).

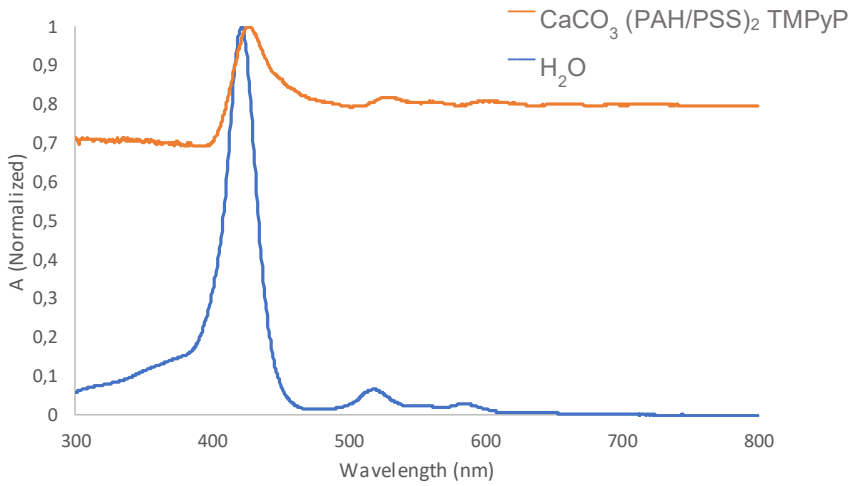

Figure 18 – UV-Vis absorbance spectra normalized of TMPyP absorbed onto polyelectrolyte microcapsules (orange) and in aqueous solution (4.9×10^{-6} M) (blue) (pH=7).

It is noticeable a small redshift (~4nm) and a broadening of the Soret band when adsorbed into the microcapsules and also a decrease in intensity relatively to both Q-bands. There is also a variation between the emission spectra of TMPyP when is free in solution and adsorbed onto polyelectrolyte microcapsules (figure 18).

The free base water TMPyP presents a characteristic emission spectrum with two vibrational bands Q (0,0) and Q (0,1) around 650 nm and 718 nm, respectively. The unresolved emission is described in literature [19]. The Q (0,0) emission band appears as a shoulder of the broad Q (0,1) band which is explained by the mixing of the first excited state of TMPyP with nearby charge transfer state due to electron transfer between the porphyrin core to the pyridinium meso-substituents. The rotational freedom of the pyridinium group determines the degree of coplanarity and resonance between the porphyrin core and pyridinium meso-substituents.

The interaction of TMPyP with PSS changes the absorbance spectra of TMPyP in solution. The maximum of the Soret band changes from 422 nm to 433 nm. The interaction with PAH is not favored and the absorbance spectrum does not change from one of the free base porphyrin. The broadening observable in the spectrum of TMPyP adsorbed microcapsules are a result of the interaction with the shell (figure 19). This interaction also promotes the resolution of the emission spectrum and allows a visible separation of the Q (0,0) and Q (0,1) band. This resolution occurs due to the modification of the degree of coplanarity of the pyridinium group and the electron transfer to the sulfonate group of PSS.

The interaction with PAH polyelectrolyte is not favored due to electrostatic repulsion. It is only visible a decrease of fluorescence intensity in the emission spectrum.

The polyelectrolyte microcapsule emission spectrum is obtained as a combination of the interaction of PSS and water, as it can be denoted by a loss in the vibrational resolution when compared to PSS alone (Figure 19b)

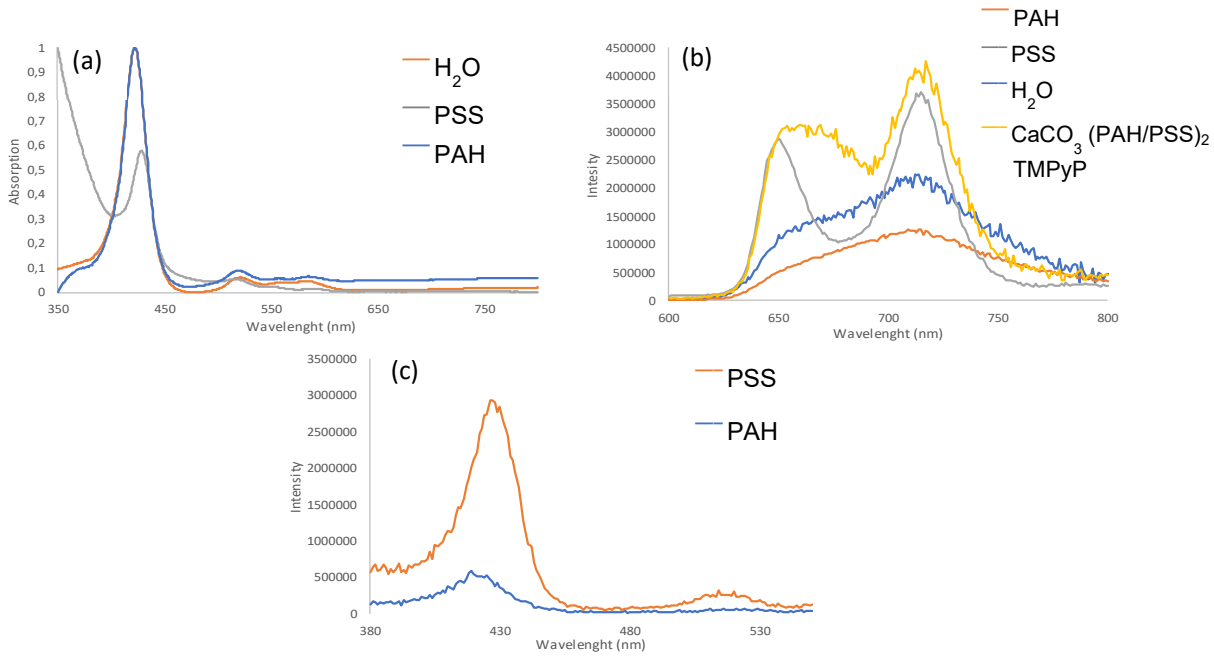

Figure 19 - UV-Vis absorption (a), fluorescence emission (λ_{exc} = 508 nm) (b) and excitation spectra (λ_{em} = 718 nm) (c) of TMPyP (4.9×10^{-6} M) in polyelectrolyte aqueous solution (3mg/ml) and adsorbed onto PECs.

It was done an excitation spectrum of TMPyP in polyelectrolyte solution, revealing a maximum at 422 nm in PAH and a maximum at 428 nm in PSS. As the PAH interaction is not favored, the excitation spectrum is overlapping with the same solution absorbance spectrum meaning that the monomeric TMPyP aqueous solution contributes to the emission in PAH. The interaction of TMPyP with PSS is favored and, by the absorbance and emission spectrum is notable this influence. In the excitation spectrum this is confirmed, being obtained a spectrum in which the maximum shifts ~6nm. In fact, this TMPyP form is the most responsible for the emission spectra and resolution.

b. Porphyrin adsorption by polyelectrolyte microcapsules: Spectroscopic studies

i. Encapsulation Efficiency

The efficiency of a drug delivery system depends on the amount of pharmaceutical that can transport. To characterize and compare our systems, it was calculated the encapsulation efficiency by UV-Vis absorbance. We started by determining the amount of porphyrin adsorbed per amount of polyelectrolyte microcapsule. For this, we measured the absorption of the supernatant of a porphyrin solution (H_2TSPP^{-4}/TMPyP, 0.3mg/ml) before and after one hour in contact with a known amount of polyelectrolyte microcapsules (figure 20). The difference found in absorption is proportional to the concentration of porphyrin adsorbed by polyelectrolyte microcapsules, accordingly with Beer-Lambert law. After separation of the supernatant from the polyelectrolyte microcapsules by centrifugation, the

microcapsules were dried in vacuum and weighed. The encapsulation efficiency was then calculated (Table 2, Annexes 1).

Table 2 – Encapsulation Efficiency of the systems studied (mean values of three experiments).

System	Encapsulation Efficiency (%)
$CaCO_3(PAH/PSS)_2PAH\ H_2TSPP^{-4}$	2.32 ± 0.06
$CaCO_3(PAH/PSS)_2\ H_2TSPP^{-4}$	0.42 ± 0.02
$CaCO_3(PAH/PSS)_2$ TMPyP	1.43 ± 0.08

The system more efficient to encapsulate porphyrin was the $CaCO_3(PAH/PSS)_2PAH$ with the higher mass of H_2TSPP^{-4} adsorbed by mass of polyelectrolyte microcapsules (Table 2). The encapsulation efficiency of this system was almost 1% higher than $CaCO_3(PAH/PSS)_2$ TMPyP and approximately six times higher than $CaCO_3(PAH/PSS)_2\ H_2TSPP^{-4}$. These results are as expected as the electrostatic interactions between opposite charged polyelectrolytes and porphyrins are favored.

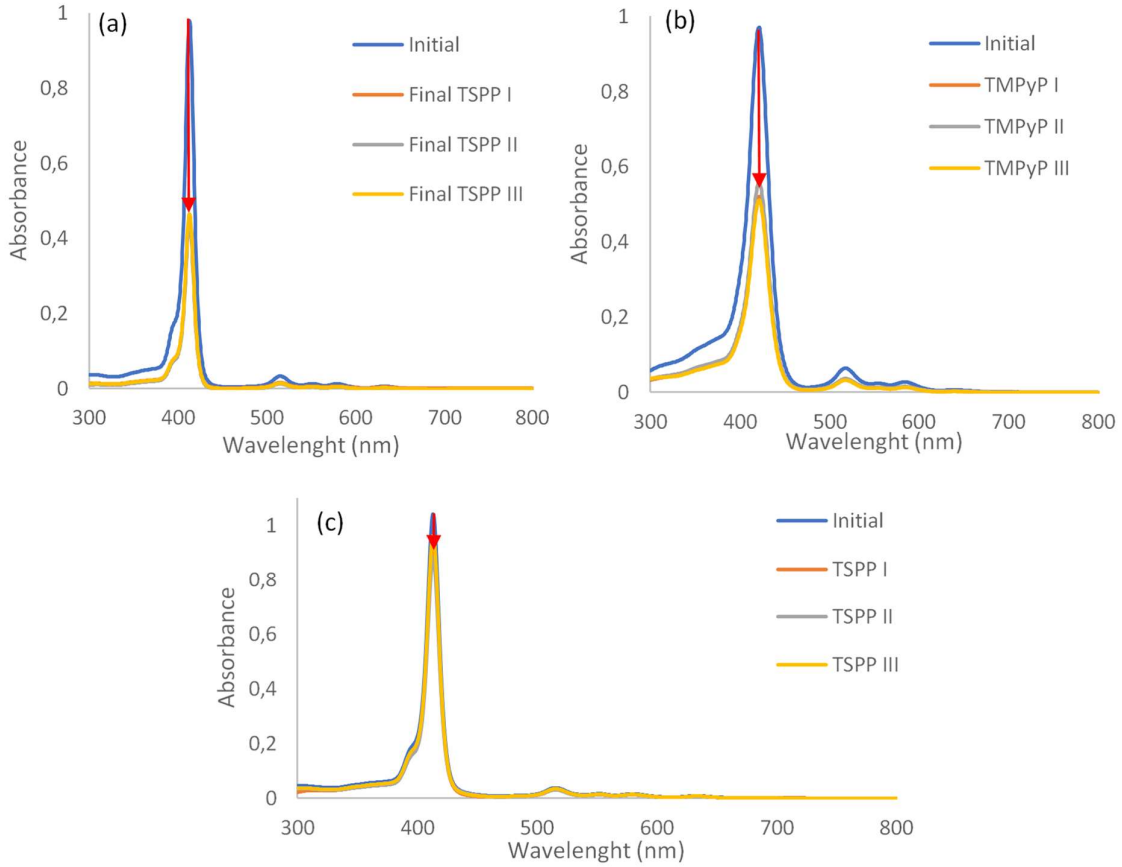

Figure 20 – UV-Vis absorbance spectra of the initial and final supernatant solutions of (a,c) H_2TSPP^{-4} and (b) TMPyP. The correspondent microcapsules systems are (a) $CaCO_3(PAH/PSS)_2$ PAH H_2TSPP^{-4} (b) $CaCO_3(PAH/PSS)_2$ TMPyP and (c) $CaCO_3(PAH/PSS)_2\ H_2TSPP^{-4}$. I, II and III refer to three independent experiments.

ii. Characterization by Fluorescence Lifetime Image Microscopy (FLIM)

FLIM measurements were also done in order to compare both systems of H_2TSPP^{-4} adsorbed in polyelectrolyte microcapsules. The polyelectrolyte microcapsules non-functionalized are non-emissive upon irradiation at λ_{exc}=635nm therefore is possible to conclude that the emission observed only arises from the adsorbed H_2TSPP^{-4}. A TEM image of the non-functionalized systems is shown in figure 21, assuring a good circular shape previous to porphyrin adsorption. Figure 22 is the FLIM image of H_2TSPP^{-4} adsorbed onto $CaCO_3(PAH/PSS)_2$ PAH polyelectrolyte microcapsules of the same sample at different scales.

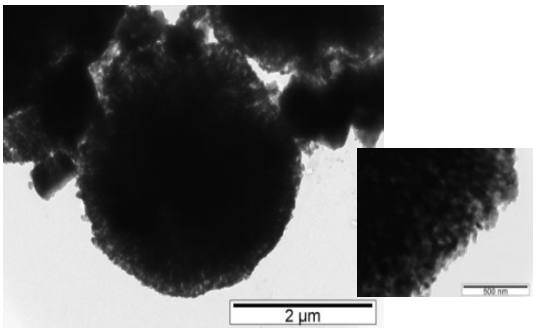

Figure 21 – TEM image of polyelectrolyte microcapsules $CaCO_3$ $(PAH/PSS)_2$ PAH.

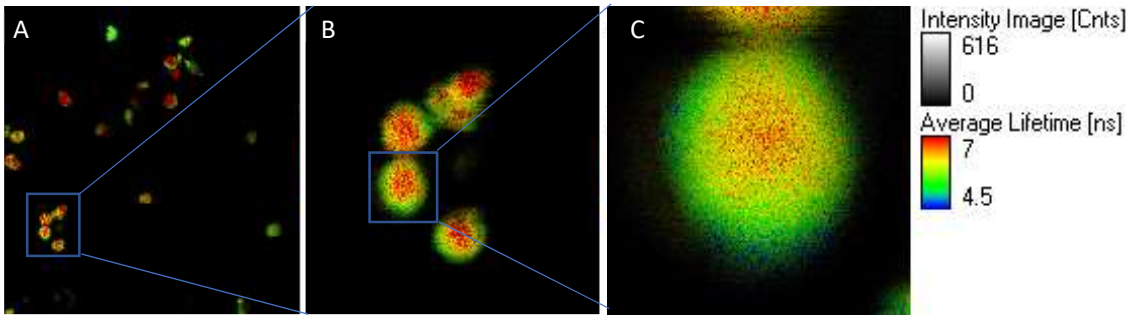

Figure 22 – FLIM of H_2TSPP^{-4} adsorbed onto $CaCO_3(PAH/PSS)_2$ PAH polyelectrolyte microcapsules. (A) 80µm^2; (B) 20µm^2; (C) 5µm^2

The intensity of H_2TSPP^{-4} fluorescence at the microcapsules depends on the form and on its location. The FLIM images obtained from the system $CaCO_3(PAH/PSS)_2PAH$ H_2TSPP^{-4} shows micrometric fluorescent rounded shapes (matrix-type) well dispersed and with the same shape as the microcapsules in the TEM study (figure 21). It also shows that H_2TSPP^{-4} diffuses into the multilayer film, from the interface to the inner core (figure 22).

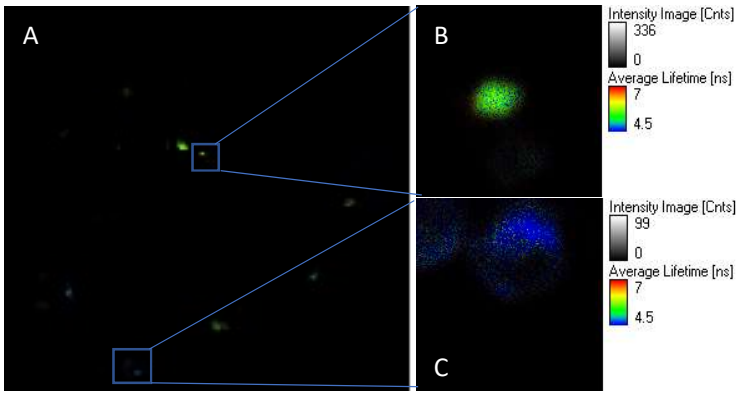

Figure 23 - FLIM of H_2TSPP^{-4} adsorbed onto $CaCO_3(PAH/PSS)_2$ polyelectrolyte microcapsules. (A) 80μm²; (B) 5μm²; (C) 5μm².

The figure 23 is the FLIM image of H_2TSPP^{-4} adsorbed onto $CaCO_3(PAH/PSS)_2$ polyelectrolyte microcapsules of the same sample at different scales. Figure 22B and 22C are both microcapsules which demonstrate a high variability of the system as different microcapsules present a different distribution of lifetimes.

The FLIM images show a less uniform system as it is only visible irregular microcapsule shapes with different range of lifetimes and it is also difficult to differentiate the core and periphery of the microcapsule. The microcapsules of the $CaCO_3(PAH/PSS)_2$ H_2TSPP^{-4} system have smaller diameters (3-3,5μm) that $CaCO_3(PAH/PSS)_2PAH$ H_2TSPP^{-4} system (4,5-5μm).

Table 3 – Fluorescence lifetimes of H_2TSPP^{-4} (pH=7) in aqueous solutions with polyelectrolytes and associated with the polyelectrolyte microcapsules.

	τ_1 (ns)	A(%)	τ_2 (ns)	A (%)	τ_3 (ns)	A(%)	τ_{avg}	$\chi 2$
H_2O*	10	100	-	-	-	-	10	1,066
PAH*	1	62	10,9	38	-	-	9,6	1,187
PSS*	3,2	62	10,5	38	-	-	7,7	1,102
$CaCO_3(PAH/PSS)_2PAH$ (a)	0,9	28,4	4,5	40,8	8,7	30,8	4,8	1,01
$CaCO_3$ $(PAH/PSS)_2PAH$ (b)	0,6	35,1	2,8	46,0	6,0	18,9	2,5	0,962
$CaCO_3$ $(PAH/PSS)_2$ (a)	0,5	52,7	3,5	27,6	9,3	19,6	3,1	1,069
$CaCO_3$ $(PAH/PSS)_2$ (b)	0,5	56,9	3,2	26,6	9,1	16,5	2,6	1,055

*[60]
(a) Core (b) Periphery

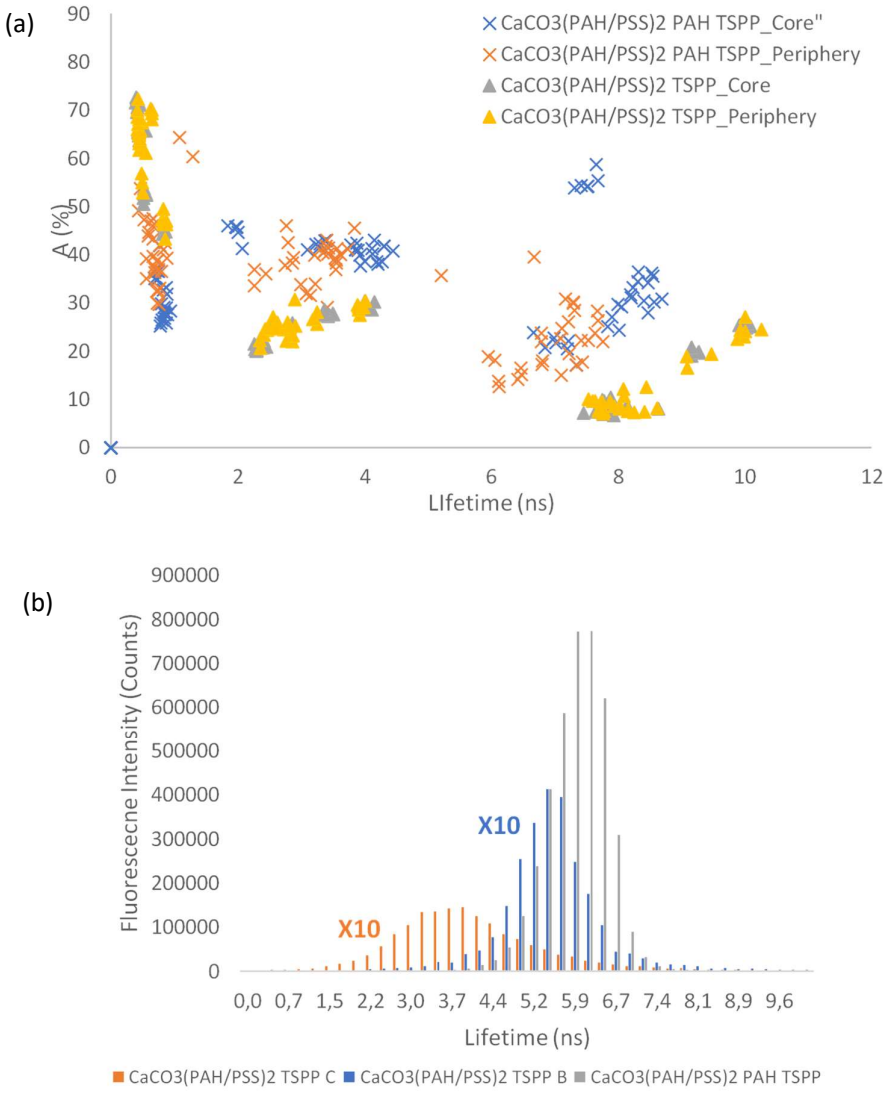

Figure 24- (a) Distribution of fluorescence lifetimes of $CaCO_3$ $(PAH/PSS)_2PAH$ H_2TSPP^{-4} and $CaCO_3$ $(PAH/PSS)_2$ H_2TSPP^{-4} in the core and periphery. (b) Histogram of fluorescence lifetimes measured in both samples.

The interpretation of the lifetime results is not straightforward. The fluorescence lifetime results of H_2TSPP^{-4} adsorbed onto PECs can be decomposed in three exponential factors (figure 24 a). The longest fluorescence lifetime (6-10 ns) can be attributed to the interaction between H_2TSPP^{-4} and the interstitial waters of the system or with PAH. The medium fluorescence lifetime (2-4 ns) can be attributed to the interaction between H_2TSPP^{-4} and PSS polyelectrolyte. The shorter lifetime (<1 ns) is of complex nature and cannot be easily attributed to a single interaction (figure 24 a; Table 3).

The histogram of the overall systems fluorescence lifetimes adsorbed with H_2TSPP^{-4} show different distributions in the $CaCO_3(PAH/PSS)_2$ H_2TSPP^{-4} system. This is in accordance with the FLIM images obtained from this system detailing its heterogeneity (figure 24b).

The results of this displacement are responsible to the differences already been discussed in the absorption, emission and excitation spectra of both systems.

FLIM measurements were also done in order understand the TMPyP system adsorbed in polyelectrolyte microcapsules. The emission observed only arises from the adsorbed TMPyP.

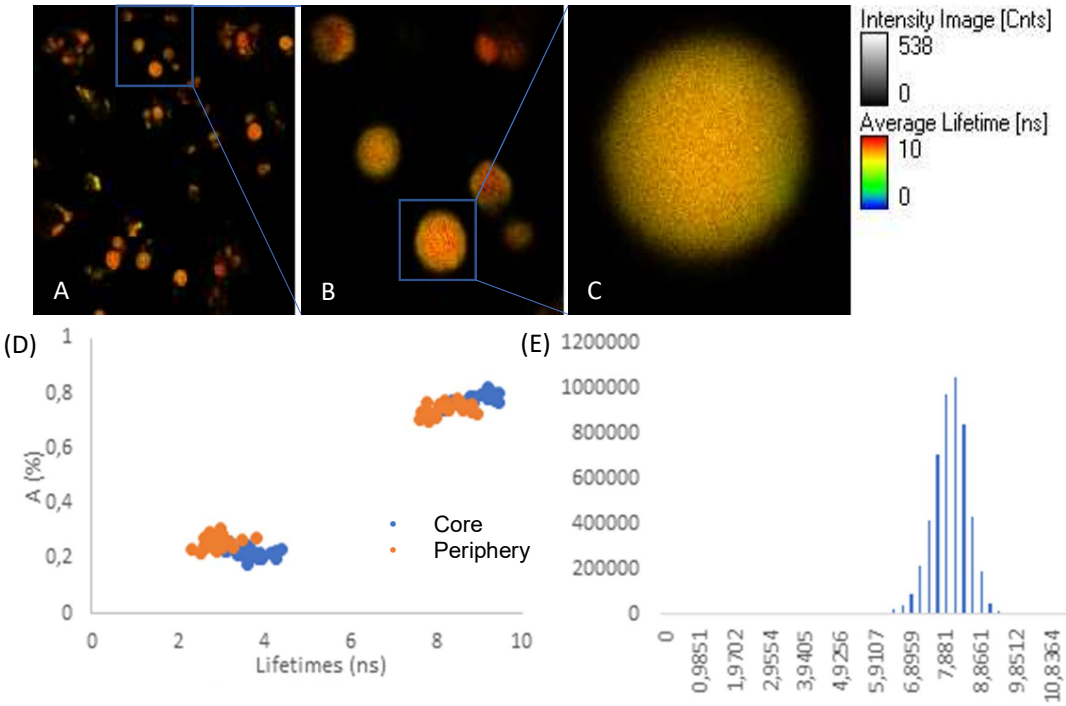

Figure 25 - FLIM of TMPyP adsorbed onto $CaCO_3(PAH/PSS)_2$ polyelectrolyte microcapsules. (A) 80μm²; (B) 13μm²; (C) 5μm². (D) Distribution of fluorescence lifetimes measured in different points of microcapsules. (E) Distribution of total fluorescence lifetimes of polyelectrolytes microcapsules.

Table 4 – Fluorescence lifetimes of TMPyP (pH=7) in aqueous solutions with polyelectrolytes and associated with the polyelectrolyte microcapsules.

	τ_1 (ns)	A (%)	τ_2 (ns)	A (%)	τ_{avg}	χ^2
H_2O	5,4	83,6	<0,01	16,4	5,3	1,18
PSS	-	-	13,8	100	13,8	1,11
$CaCO_3$ $(PAH/PSS)_2$ (a)	3,1	23,2	8,3	76,8	7,1	1,11
$CaCO_3$ $(PAH/PSS)_2$ (b)	2,6	27,2	7,7	72,8	6,3	1,05

(a) – Core (b) – Periphery

The FLIM images show fully doped polyelectrolyte microcapsules with round shapes well dispersed (matrix-type) and a very homogenous system (figure 25A,B and C) For the measure of fluorescence lifetimes, the measures revealed complex decays in which two exponential components were always needed to achieve a proper fit.

It is observable a shorter distribution of fluorescence lifetimes (2-4 ns) with a lower contribution that can be attributed to the interaction between TMPyP and the interstitial waters of the system. The longer distribution of fluorescence lifetimes (8-10 ns) with a higher contribution can be attributed to the interactions between TMPyP and PSS. (figure 25D and Table 4).

The overall fluorescence lifetime histogram revealed a homogeneous distribution of fluorescence lifetimes (figure 25E).

The fluorescence lifetime distribution of the polyelectrolyte microcapsule systems adsorbed with porphyrin were obtained by FLIM. Is possible to observe, by fluorescence lifetimes, the different interactions that rises in the system specially between the porphyrin and the polyelectrolyte multilayer film. Instead of a simple adsorption on the surface of the polyelectrolyte microcapsules, the results show that occurs a diffusion of the porphyrin inside the system whose presence is possible in complexed form with polyelectrolyte or in the interstitial waters.

CHAPTER 5

Porphyrin release

As it has already been discussed, the photodynamic therapy efficiency shows a great dependence on the local concentration of photosensitizer and one of the ultimate goals of this study is to understand if the polyelectrolyte microcapsules may work as an efficient porphyrin delivery method. As the adsorption of porphyrin has already been studied, is important to understand how the system behaves in controlled environments that mimic different parts of the human body. $CaCO_3(PAH/PSS)_2$ PAH H_2TSPP^{-4}, $CaCO_3(PAH/PSS)_2$ H_2TSPP^{-4} and $CaCO_3(PAH/PSS)_2$ TMPyP systems were studied.

a. Intestinal environment

i. H_2TSPP^{-4} and TMPyP release

For this release, it was used the intestinal solution (pH=7.2, 0.68% (w/v) KH_2PO_4), with the objective to mimic pH neutral and intestinal environments.

Table 5 – Total amount of porphyrin release and % Release observed for polyelectrolyte microcapsule in intestinal environment

System	H_2TSPP^{-4}/TMPyP release (µg)	% Release
$CaCO_3(PAH/PSS)_2PAH$ H_2TSPP^{-4}	1,63	2,18
$CaCO_3(PAH/PSS)_2$ H_2TSPP^{-4}	0,04	0,92
$CaCO_3(PAH/PSS)_2$ TMPyP	0,87	1,98

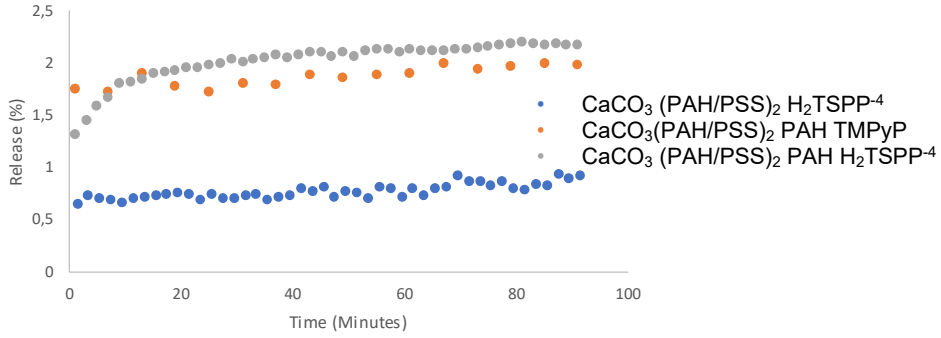

Figure 26 - Porphyrin release from $CaCO_3(PAH/PSS)_2PAH$ H_2TSPP^{-4}, $CaCO_3(PAH/PSS)_2$ H_2TSPP^{-4} (λ_{exc}=413 nm; λ_{emi}=650 nm) and $CaCO_3(PAH/PSS)_2TMPyP$ in intestinal environment. (λ_{exc}=421 nm; λ_{emi}=718 nm).

It's observed that the system $CaCO_3(PAH/PSS)_2PAH$ H_2TSPP^{-4} is the system that has the higher amount of H_2TSPP^{-4} released in the solution. Nevertheless, this quantity is very low (~2.18%) comparing with the overall amount of H_2TSPP^{-4} that has been adsorbed in the polyelectrolyte microcapsules. $CaCO_3$ $(PAH/PSS)_2$ TMPyP release values were near the release percentage of $CaCO_3(PAH/PSS)_2PAH$ H_2TSPP^{-4}. In the system $CaCO_3(PAH/PSS)_2$ H_2TSPP^{-4} the release values were very low (~1%) (figure 26, table 5).

The sustained release of porphyrin in a neutral pH environment is not very effective which means that has a high stability when travelling inside the human body in this type of environment. If the release is done inside a cell and the pH values are not acidic, the porphyrin release is very low. Since

the release studied does not incorporate all the cell conditions it is possible that due to the biological or mechanical mechanisms present in cell, such as enzyme activity or endocytosis, the polyelectrolyte microcapsules degrade and give way to a burst release yielding a higher release efficiency.

The system $CaCO_3$ $(PAH/PSS)_2$ H_2TSPP^{-4} yield the lowest release in these conditions. Therefore, the interest of the release kinetics in other conditions are only being studied for the $CaCO_3(PAH/PSS)_2PAH$ H_2TSPP^{-4} and $CaCO_3$ $(PAH/PSS)_2$ TMPyP system.

To further understand the H_2TSPP^{-4} release conditions, the release was studied for longer time while renewing the intestinal release solution (Figure 27).

Table 6– Release of H_2TSPP^{-4} in intestinal conditions and supernatant fluorescence emission measured after 30 and 300 minutes (with medium renewed).

Time (Minutes)	Release H_2TSPP^{-4} (µg)	Release H_2TSPP^{-4} (%)
30	1,52	1,98
420	3,39	4,41

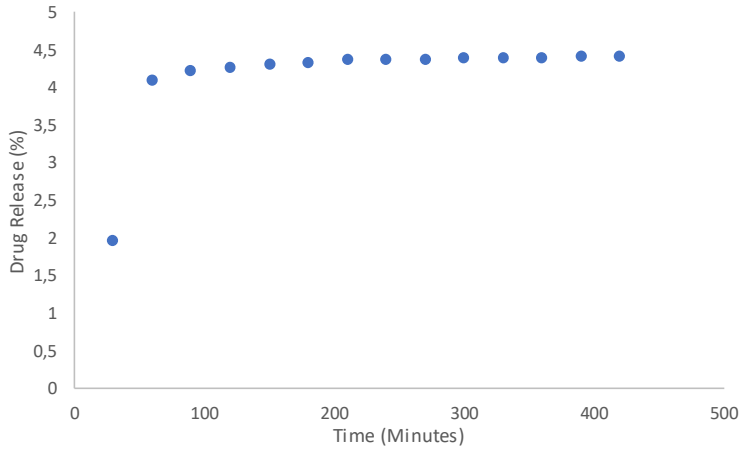

Figure 27 –Release profile (%) of $CaCO_3$ $(PAH/PSS)_2PAH$ H_2TSPP^{-4} (λ_{exc}=413 nm; λ_{em}=650

With the continuation of the H_2TSPP^{-4} release in intestinal conditions is possible to infer that the release is fast in beginning but it tends to stabilize its release without the system being completely clear of H_2TSPP^{-4} (table 6). It reveals a system that tends to stabilize its release after a long time in a neutral pH environment.

b. Gastric environment

For this release, the objective was to mimic the stomach environment (pH=2.0, 0.2% (w/v) NaCl).

One problem that was reported when the release study was done in acidic pH was that the low pH degrades the $CaCO_3$ core of the polyelectrolyte microcapsules. This promotes the core degradation and a neutralization of the environment pH (Annexes 2) causing oscillating inflating-deflating cycles due

to CO_2 formation and release, promoting the capsule collapse. Its believed that this effect promotes the higher porphyrin release but also the release of polyelectrolytes to the supernatant as the destruction of the capsule occurs. Another side effect is that polyelectrolyte microcapsules do not have enough weight to stay in the bottom part of the cuvette, therefore, they rise due to the stirring motion affecting the release kinetics measures and increasing the measure of the release efficiency.

Due to the error imposed in the release kinetics measuring, only the supernatant measured after centrifugation and removal of the microcapsules, is used for the calculation of the release of porphyrin by polyelectrolyte microcapsules in this environment.

i. H_2TSPP^{-4} Release

When the fluorescence emission of the supernatant solution is measured, the shape of the emission spectrum is similar to the spectrum of H_2TSPP^{-4} at pH 7.0 rather than the emission spectrum of the acidic form H_4TSPP^{-2}. The kinetics was followed by picking the 650nm wavelength (figure 28).

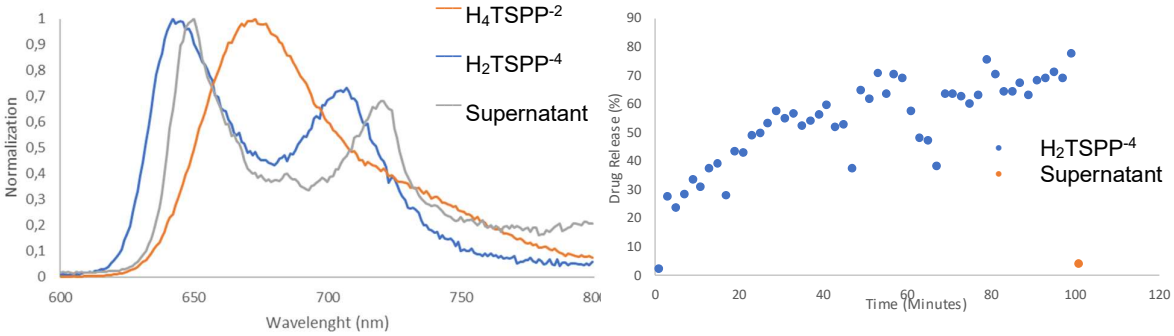

Figure 28 – (a) Emission spectra of H_2TSPP^{-4}, supernatant solution after the release at pH 2.0. (λ_{exc}=413 nm) and H_4TSPP^{-2} (λ_{exc}=434 nm) spectrum (b) Release profile of $CaCO_3(PAH/PSS)_2PAH$ H_2TSPP^{-4} in gastric environmental conditions (blue) and respective supernatant after removal (orange) (λ_{exc}=413 nm; λ_{em}=650 nm).

The emission spectrum reveals that the environment pH, during the release, is not acidic as the H_4TSPP^{-2} emission spectrum at an acidic pH is only comprised by one broad band (675 nm) and the supernatant emission spectra is similar to the H_2TSPP^{-4} emission spectrum at pH 7.0. The slight red-shift is characteristic with the interaction with PAH which opens the possibility that due to the core destruction, the oscillating inflating-deflating cycles due to the CO_2 formation and the polyelectrolyte microcapsules collapse, H_2TSPP^{-4} is released in a complex with PAH.

It is visible the difference in values during the kinetic measuring and after the separation of the polyelectrolyte microcapsules and supernatant measure. As already stated, this difference is due to the presence of polyelectrolyte microcapsules in the kinetics solution as the low stirring velocity is enough to suspend the now-hollow polyelectrolyte microcapsules as an effect of the destruction of the core.

Due to the high variability observed, only the supernatant measured was accounted for the calculations of the release efficiency (Table 7).

As the neutralization of the pH environment value occurs and has an impact on the release kinetics it is necessary to understand the release kinetics when the pH is still 2.0. For this, the study of the release was performed switching the release solution for a fresh one in periods of thirty minutes in order to achieve optimal release conditions (figure 29).

Table 7 – Release of H_4TSPP^{-2} and supernatant fluorescence emission measured after 30 and 300 minutes (with medium renewed).

Time (Minutes)	Release H_4TSPP^{-2} (ug)	Release H_4TSPP^{-2} (%)
30	2,55	4,10
300	54,48	87,72

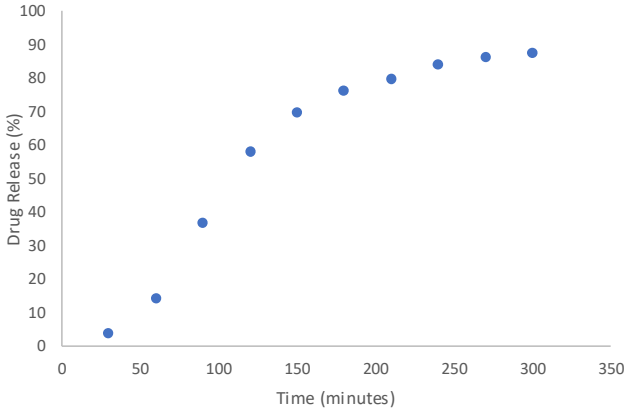

Figure 29 –Release profile (%) of $CaCO_3$ $(PAH/PSS)_2PAH$ H_2TSPP^{-4} (λ_{exc}=413 nm; λ_{em}=650 nm).

With the renewal of the gastric release solution is possible to notice the continuum porphyrin release due to the acidic pH conditions. This release achieved 87.72% over the total H_2TSPP^{-4} that was adsorbed initially in the polyelectrolyte microcapsules as the reduction of the reddish tone of the polyelectrolyte microcapsule was observable along the release kinetics finishing without any red color precipitate.

Is possible to conclude with this result that if the medium in which the polyelectrolyte microcapsules are is not neutralized (stomach conditions) a high release of H_2TSPP^{-4} is inevitable after more than five hours.

ii. TMPyP release

The release of TMPyP from polyelectrolyte microcapsules also yield the same phenomena of the release of H_2TSPP^{-4} at an acidic pH. These phenomena are due to the destruction of the $CaCO_3$ core giving rise to the neutralization of the medium and destruction of the polyelectrolyte microcapsules increasing the variability of the kinetics measures and adding a large error to the fluorescence emission values. For the calculation of the release efficiency, the supernatant value after centrifugation was the only accounted for.

It was observed that the first half hour of the reaction resulted in a high concentration of TMPyP released. Due to inner filter effects (A > 0.2) which limits spectrofluorometer measures, the release of TMPyP was followed by the emission spectrum (718 nm) when excited at 508 nm (TMPyP Q-band) rather than being excited at 421 nm (TMPyP Soret band).

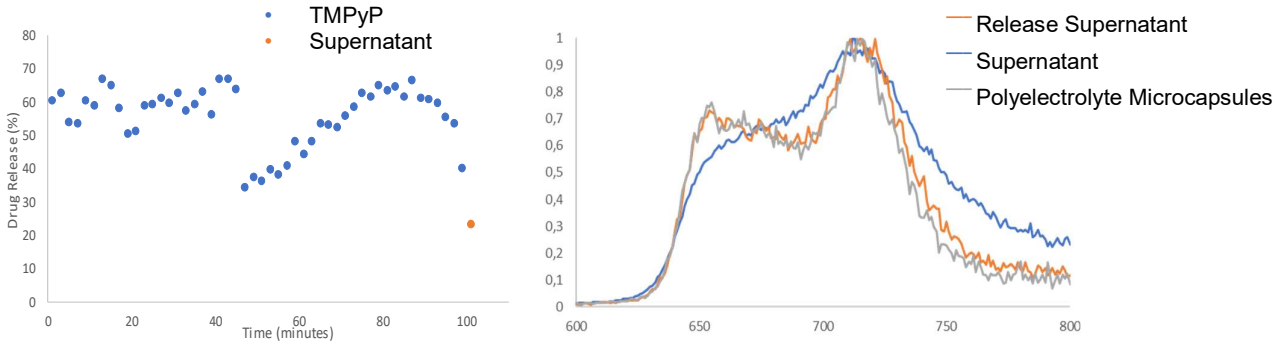

Figure 30 - (a) Release profile of $CaCO_3(PAH/PSS)_2$ TMPyP in gastric environmental conditions (blue) and respective supernatant after removal (orange) (λ_{exc}=508 nm; λ_{em}=718 nm). (b) Emission spectra of TMPyP in supernatant, TMPyP emission spectra during the kinetics and the polyelectrolyte microcapsules after the release of TMPyP at pH 2.0.

The differences in fluorescence intensity observed between the supernatant after removal and previous to removal (during release measurements) are very different. The last, seems to have a high influence from the presence of microcapsules. It was believed that due to the destruction of the polyelectrolyte microcapsules, TMPyP was released in a complex form with PSS although this was not possible to be confirmed as the centrifugation stage has possibly removed the polyelectrolyte complex or the remaining polyelectrolyte microcapsules (figure 30).

Due to the neutralization of the medium pH, it was found interesting to continue the release kinetics while changing the medium, in order to study the continuous release of the system in acidic pH without interference from the change in pH.

For this, the polyelectrolyte microcapsule system adsorbed with porphyrin was left in a release solution, the medium was changed in periods of thirty minutes and the fluorescence emission spectrum of supernatant was measured (figure 31).

Table 8 – Release of TMPyP and supernatant fluorescence emission measured after 30 and 300 minutes (with medium renewed).

Time (Minutes)	Release TMPyP (µg)	Release TMPyP (%)
30	9,32	23,40
450	18,72	47,00

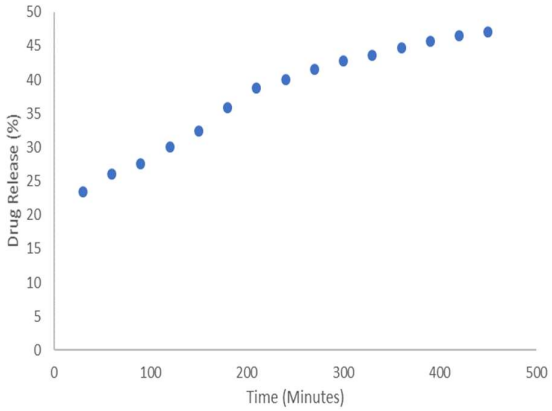

Figure 31 - (a) Release Kinetics measured by fluorescence emission along time and (b) Porphyrin Release (%) of the overall polyelectrolyte microcapsules sample along time (λ_{exc}=421 nm; λ_{em}=718 nm)

In gastric pH conditions, the polyelectrolyte microcapsules adsorbed with TMPyP have a higher release in the first thirty minutes when compared with the H_2TSPP^{-4} system (table 8). Nevertheless, it still continues to have the possibility for some release even after eight hours. This reveals that the system endures more time in gastric conditions when compared with H_2TSPP^{-4} absorbed in polyelectrolyte microcapsules.

c. Light-Mediated Release

The sustained release studies done in different conditions (intestinal and gastric) showed the continuous response of polyelectrolyte microcapsule system to the environment. Light-mediated burst release was found interesting to study in this system due to the presence of a fluorophore and to study the impact of light irradiation on the polyelectrolyte microcapsule system.

Previous works already showed light mediated degradation of polyelectrolyte microcapsules functionalized with H_2TSPP^{-4} but only with H_2O_2 present in solution [47]. Nevertheless, the possibility to further control the release of polyelectrolyte microcapsules functionalized with a porphyrin, mediated by a remote and physical method opens a new pathway for controlled release inside the target tissue, increasing the local concentration of porphyrin and increasing the PDT efficiency.

Due to the higher encapsulation efficiency and release in intestinal conditions, the $CaCO_3$ $(PAH/PSS)_2$ PAH system with adsorbed H_2TSPP^{-4} was selected.

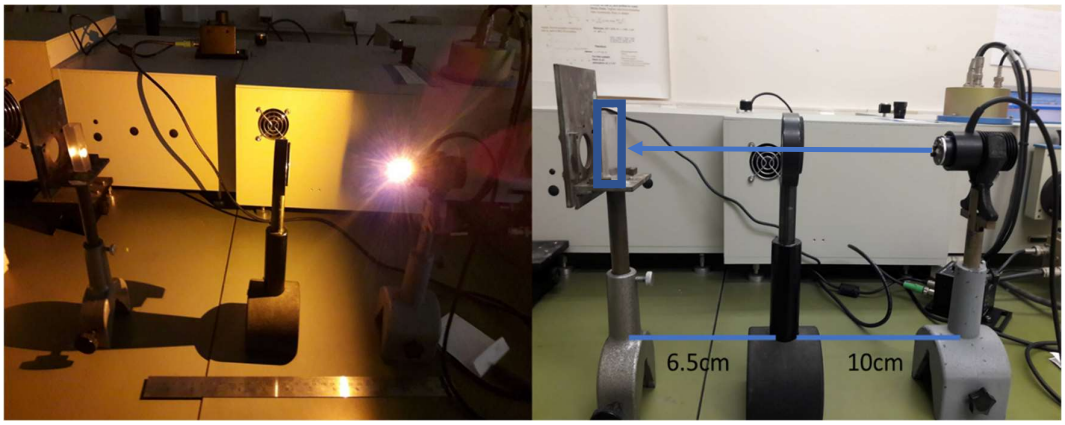

Figure 32 – Assembly of the light-mediated release device. The light travels from the laser source and is focused ending irradiating the system. After light irradiation, the supernatant fluorescence emission is measured. The area of irradiation has a radius of 1.5cm.

Following the scheme of figure 32, the system was irradiated by a laser with 0.5mW/cm^2 of irradiance power at 595 nm. After periods of two minutes, the fluorescence emission was measured and the release profile was evaluated at 650 nm. This kinetic was done in intestinal conditions.

The light-mediated release was compared with the release in intestinal conditions without light irradiation of the same system for easier understanding the light effects on the polyelectrolyte microcapsule system (Figure 33).

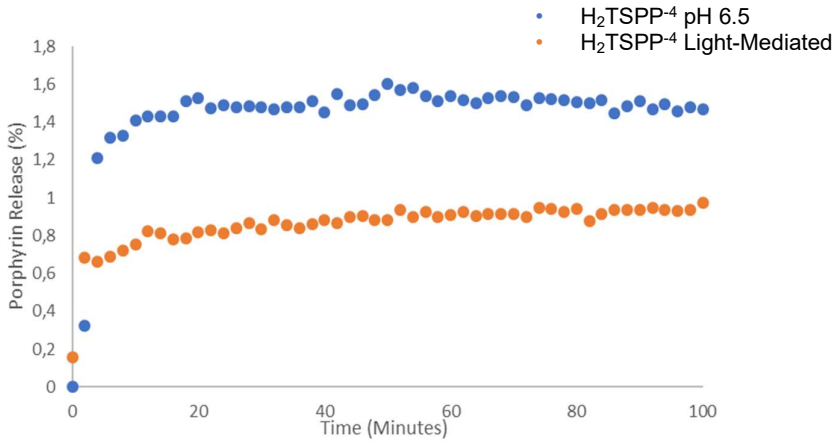

Figure 33 – Fluorescence emission measured for $CaCO_3(PAH/PSS)_2PAH$ TSPP in intestinal condition with (orange) and without (blue) light irradiation (λ_{exc}=413 nm; λ_{em}=650 nm).

The release of polyelectrolyte microcapsules in intestinal conditions without light irradiation actually yield a release of 1.5% while the light mediated release in the same conditions yield a lower release of 0.9%.

To confirm the lower light-mediated release of H_2TSPP^{-4} from polyelectrolyte microcapsules, is important to confirm that there is not any degradation or photobleaching of H_2TSPP^{-4} when irradiated by the laser (Figure 34).

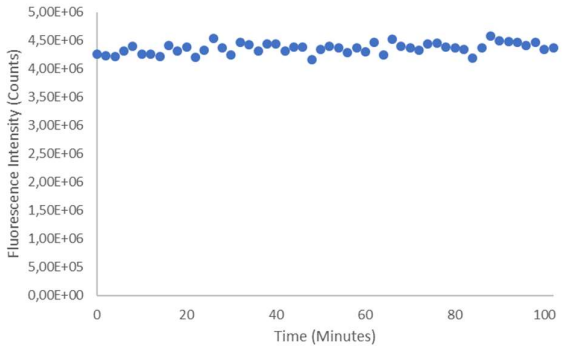

Figure 34 – Fluorescence emission of H_2TSPP^{-4} (c = $2.14x10^{-4}$mM) that has been irradiated in the same conditions of the light-mediated release.

The light irradiation of H_2TSPP^{-4} did not have enough intensity to degrade the porphyrin. This means that the release in intestinal conditions was higher without any light irradiation than in a light-mediated release, so the light irradiation actually hinders the H_2TSPP^{-4} release.

Some possibilities are opened to why the light-mediated release actually hinder the H_2TSPP^{-4} release form the polyelectrolyte microcapsule system. These are: low irradiance power from the LED, formation of cross-linking bonds between the polyelectrolyte network and not enough oxidative environment (Bédard *et al.* actually added H_2O_2 to the solution in order to achieve microcapsule destruction [47]).

These results are actually contrary of what was expected but although the release has affected and cannot be used as a remote physical burst release method, it also shows that following the polyelectrolyte microcapsule delivery can be possible without compromising the drug delivery process, as the tracking of the system actually does not destroy it. It maybe still possible that if the formation of oxidative species by the polyelectrolyte microcapsules inside the cancer tissue is high enough, a light trigger can also ensure the complete release of the load by destruction of the delivery vehicle.

d. Conclusions

The use of the polyelectrolyte microcapsules as drug delivery systems shows a high stability of the system in neutral pH conditions adequate for drug transport in human body systemic circulation. The best therapeutic effects due to higher release values can be obtained in stomach cancer. Accompanied by destruction of $CaCO_3$ core, neutralization of the medium is verified (Annexes 2).

A triggered remote release of the system was not achieved using light, possibly only occurs in already high oxidative environments.

CHAPTER 6

Core-assisted formation of porphyrin J-aggregates in pH- sensitive polyelectrolyte microcapsules.

In an attempt to improve the porphyrin loading onto polyelectrolyte microcapsules, we thought in adsorbing H_2TSPP^{-4} in its dianionic form (H_4TSPP^{-2}) and compare the results with the ones previously obtained using an adsorption solution of tetraanionic H_2TSPP^{-4} (Chapter 4). With this idea in mind, we have studied the pH effect on porphyrin adsorption efficiency using UV-Vis absorption spectroscopy.

Interestingly we have found evidences for the growth, on microcapsules microenvironment, of different self-assembled structures, which were further identified as J aggregates. We have also observed that the formation, size and homogeneity of these aggregates are highly dependent on the pH either of adsorption solution or the surrounding environment as well as on the stirring conditions.

Regarding the potential application of porphyrins in PDT, aggregate species present several disadvantages when compared to monomers. The most important one is the significant reduction of the intersystem crossing yield, leading to low triplet state efficiencies, which is the initial state for singlet oxygen formation. In such a way, the formation of the cytotoxic species is meaningfully reduced and the photodynamic activity clearly compromised. Additionally, lower fluorescence quantum yields are also a result of porphyrin aggregation [61]. Even though the formation of porphyrin J-aggregates in solution and in confined environments has been widely studied, in the last decade due to their attractive applications in optoelectronics, that makes it an active area of research, their formation in polyelectrolyte microcapsules is almost unknown.

Information on the possibility of porphyrin aggregation in core-shell polyelectrolyte microcapsules may be useful to the knowledge of these systems properties and applicability. We decided to go a step forward and study in detail the aggregation phenomena observed. UV-Vis absorption, steady-state and transient emission and Fluorescence Lifetime imaging microscopy (FLIM) were the main spectroscopic and microscopic techniques used for their optical and morphological characterization. A new methodology to promote the organized self-assembly of H_2TSPP^{-4} on pH sensitive core shell polyelectrolyte microcapsules systems of PSS and PAH was developed using mild pH conditions (pH 3).

First, a general overview and description of porphyrin aggregates is presented, covering some already reported work regarding their formation in nano- and micro-confinement. Afterwards, the experimental results will be presented and discussed obtained highlighting their potential future applications.

a. Porphyrin Aggregates: General Overview

Much attention has been given on developing suitable conditions for the formation of nanostructured self-assembled nanostructures, which are expected to have important applications for the development of new technologies. Often, these are inspired by light harvesting complexes and reaction centers of photosynthetic organisms in order to mimic the highly efficient electron and energy transfer processes [62].

The design of assemblies based on porphyrinoids, which display a rich variety of photonic properties has remained a challenge. The main problems faced are the control of the molecular orientation and to overcome the lack of robustness due to the weak intermolecular forces involved that prevent their easy incorporation into devices [63,64]. The effective noncovalent synthesis requires a wide range of interactions, such as hydrogen bonding, electrostatic, van der Waals and hydrophobic interactions, to build well-defined supramolecular assemblies.

The excitation of molecular aggregates results in emission dynamics that are different from isolated molecules due to the formation of Frenkel excitons. These excitons are delocalized as a result of intermolecular coupling between molecules and the sharing of excitation gives rise to aggregates with electronic and spectroscopic properties that are unique [27]

The specific types of aggregates that may result due to the ionic self-assembly can be of two types: H- and J-aggregates (Figure 35) [17].

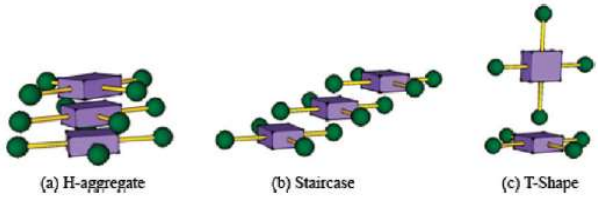

Figure 35 – Structural models for porphyrinoids (a) H- and (b,c) J-Aggregates [6]

The H-aggregates correspond to the face-to-face stacking of the monomeric species that has a blue-shift (hypsochromic) in their spectral band with respect to the absorption band of the monomer. The J-aggregates correspond to edge-by-edge or side-to-side assemblies that produce red-shifts (bathochromic) regarding the monomer absorption band [65].

The structure and photophysical proprieties of aggregates determinate their applications, for example, organic semiconductors at the nanometer scale, photovoltaic cells, artificial light-harvesting systems and nonlinear optic materials can be obtained. It has already been shown that the photocatalytic activity of porphyrin aggregates depends on their morphology. Significantly higher photocatalytic activity was observed in nanofibers of 5,10,15,20-tetra(4-pyridyl)-21H,23H-porphine compared with nanospheres of the same porphyrin, both prepared with the same methodology [66]. Bera *et al*. [67] observed a 1,9-fold increment, due to electron transfer, on the photocurrent generated under visible light from a system made of 5,10,15,20-tetrakis(4-carboxyphenyl) porphyrin nanorods (TCPP NR) and reduced graphene oxide (RGO).

Sadavisin *et al.* [68] studied the self-aggregation of a tetraanionic porphyrin on hollow microcapsules comprised of heat-sensitive multilayers made of strong polyelectrolytes (HPECs). In their approach, porphyrin self-assembly was promoted by increasing the concentration of salt and acid on the system. Satellite-like structures of HPECs containing cylindrical nanotubes protruding were isolated from the nanotubes formed in solution and were characterized by conventional spectroscopic and microscopic techniques. The aggregates dimensions were dependent on the temperature, interestingly the surface charge of the microcapsules had no impact on the orientation of the nanotubes.

The promising properties of self-assembled porphyrinoid systems and the advantages of micro and nanoconfinement, peaked the groups interest focusing on the development of photoactive polyelectrolyte microcapsules through its functionalization with porphyrin aggregates [26].

One of the most promising porphyrins for self-assembly is H_2TSPP^{-4} due to its zwitterionic character over a wide range of pH. Under acidic conditions, a combination of intermolecular ionic interactions and H-bonding between porphyrin anionic sulfonate groups and the positively charged macrocycle core of neighbour molecules are considered the main instigators for self-assembly [69]. Alterations in the absorption spectra, quantum yields, fluorescence lifetimes, and triplet state lifetimes are induced by changes in the porphyrin symmetry [70]. At pH 4.5 it is observable a symmetry change from D_2h to D_4h and a red shift in the Soret band from 413 to 434 nm accompanied by the disappearance from four to two, Q bands. Aggregation is also a fundamental state phenomenon as it changes the typical absorption spectra of porphyrins. The appearance of a red-shift peak at 490 nm and a broadband at 708 nm is assigned to monomer self-assembly towards a J-aggregate organization [71]. A broad band near 400 nm is characteristic of H-aggregation phenomenon.

b. Interaction of H_4TSPP^{-2} with PECs: Influence of the Core

The optical and electronic properties of H_4TSPP^{-2} adsorbed in PECs were studied at pH 3.0 and 1.5. These pH values were chosen with the basis on the already observed formation of J-aggregates in PAH polyelectrolyte (pH = 3.0) or in aqueous solution (pH near 1). The effect of the charge of the last polyelectrolyte layer was also evaluated.

i. pH 3.0

The core-shell polyelectrolyte microcapsules were left in contact (overnight, room temperature, with no stirring) with an aqueous solution of H_2TSPP^{-4} at pH 3.0. In this procedure, it is promoted the adsorption of porphyrin in the form of the aggregate precursor.

UV-Vis absorption was used to check the absence of J-aggregates in the adsorption solution before and after 24 hours reveling the stability of the H_4TSPP^{-2} monomer in water (TFA, pH3). Afterwards, the supernatant was removed and the polyelectrolyte microcapsule were washed with distilled water (pH 3.0). UV-Vis absorption spectra of supernatant and of core-shells microcapsules left in contact with H_4TSPP^{-2} at pH 3.0 are shown in Figure 36.

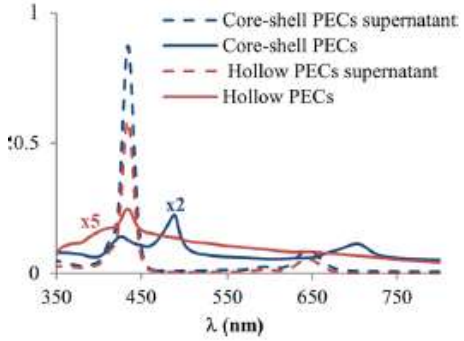

Figure 36 – UV-Vis absorption spectra of the supernatant and polyelectrolyte microcapsules of both systems (Core-shell and hollow microcapsules).

According to these results, is possible to notice the characteristic J-aggregate absorption band at 490 nm and an additional one at 708 nm, in the core-shell polyelectrolyte microcapsules. As there is no evidence of these bands in the supernatant solutions is possible to infer that the formation of J-aggregates occurs only in the core-shell microcapsule environment.

Based on previous work done in the group involving the spectroscopic evaluation of the interaction of H_4TSPP^{-2} with aqueous solutions containing different concentrations of PAH that shows clearly the formation of J-aggregates [26] we were tempted to predict that strong Coulombic attraction between the external PAH layer and the porphyrin substituents and the electrostatic interaction between neighboring molecules were the main forces to stabilize and prompt the J-aggregate growth. To evaluate this possibility, the same experience was performed after core removal. The hollow polyelectrolyte microcapsules obtained (also with PAH external layer) show different optical features (Figure 36). As can be seen, the typical absorption band of J-aggregate (490nm and 708nm) are absent in the absorption spectra and in the supernatant of the hollow polyelectrolyte microcapsules obtained in the same experimental conditions that the core-shell polyelectrolytes. In this case, only the typical monomer band (434 nm) is observed.

These observations go against the previous hypothesis, pointing to an inductive effect provided by the $CaCO_3$ presence.

The differences observed between polyelectrolyte microcapsules (Hollow or Core-shell) and the studies in solution seem to be induced by a change in the PAH/porphyrin affinity. The different Coulombic contributions between the available PAH binding sites in water and in the polyelectrolyte shell are responsible for these differences.

This is reinforced by low affinity of H_4TSPP^{-2} for the shell by analysis of the absorption spectra of H_4TSPP^{-2} adsorbed onto hollow polyelectrolyte microcapsules. Other change that clarifies this phenomenon is related with the change of the porphyrin configuration that occur upon protonation, a result of the twisting of the phenyl aryl groups from out of the plane to coplanar configuration with the porphyrin core. This coplanar configuration, the zwitterionic character of the porphyrin, the strong interpenetration of the polyelectrolyte layers on the shell adsorbed on the CaCO3 core can provide a balance between electrostatic interactions and decrease in the impact of the electrostatic repulsion. This way, the porphyrin diffusion through the water interpenetrating channels and through the charged polyelectrolyte network may be facilitated independently of the polyelectrolyte charge or presence/absence of the $CaCO_3$ core.

The spectroscopic evidence of the important role of the $CaCO_3$ core in the formation of J-aggregates was not observed after the H_4TSPP^{-2} adsorption onto the $CaCO_3$ core. In such a sense, the preferential formation of J-aggregates in the core-shell microcapsules do not rely only in the effect of the $CaCO_3$ core but on a cooperative or synergistic effect of the polyelectrolyte network.

FLIM measurements were done in order to obtain further insight into the electronic properties/morphology of the systems in the presence and absence of the core. The FLIM images (Figure 37) of the core-shell and hollow polyelectrolyte microcapsules show micrometric fluorescent round shapes that are well dispersed in solution (data not shown).

A FLIM image was also obtained for a drop of the adsorption solution. This H_4TSPP^{-2} at pH 3.0 has an average fluorescence lifetime distribution associated with its image (Figure 37A)

In Figure 37B is shown an image of a hollow polyelectrolyte microcapsule with a well-distributed fluorescence around all of the microstructure due to porphyrin adsorption and where is possible to observe that H_4TSPP^{-2} can diffuse through the polyelectrolyte complex. Its average fluorescence lifetime is centered at 5,8ns which is greater than fluorescence lifetime acquired for the H_4TSPP^{-2} droplet. It is believed that the difference in these values is related with the interaction of the porphyrin with the polyelectrolyte shell. FLIM images obtained for other aleatory chosen hollow polyelectrolyte microcapsules of the same sample shows different fluorescence lifetimes distributions, revealing a high heterogeneity within this system.

On the contrary, FLIM images obtained for core-shells polyelectrolyte microcapsules show high homogeneity within their morphology and fluorescence lifetime profiles. It also shows fluorescent micrometric circular structures with radially distributed needlelike structures protruding from the polyelectrolyte microcapsules. These structures are within the diffraction limit (ca.350nm). The fluorescence lifetimes associated with this image much shorter than the ones obtained for H_4TSPP^{-2}, a consequence expected for the aggregation phenomena.

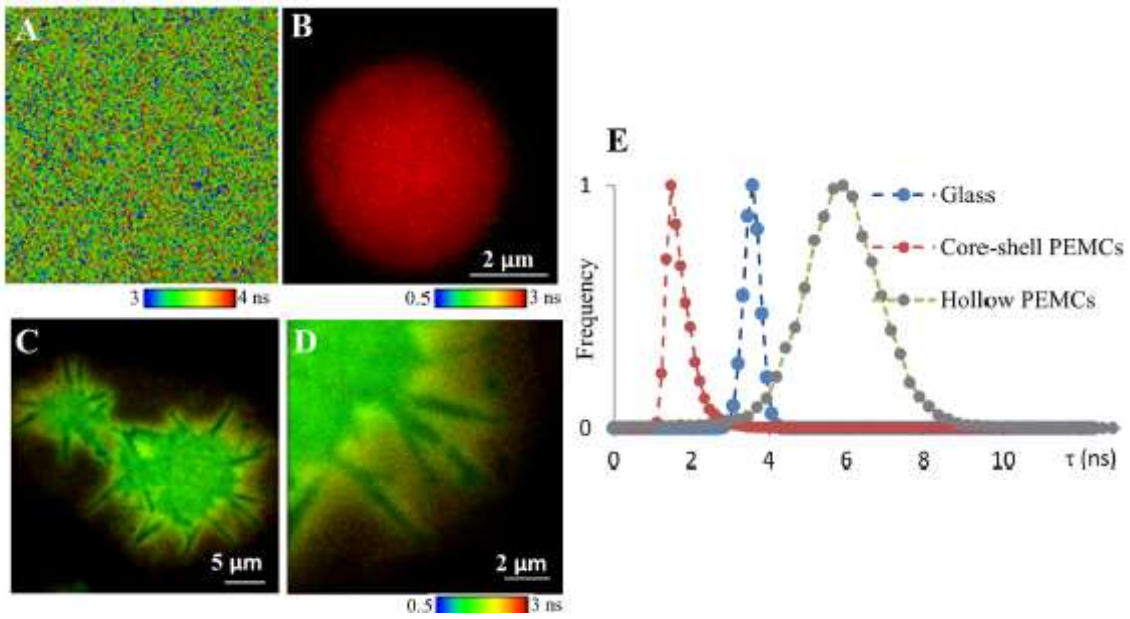

Figure 37 – FLIM images obtained of (A) H_4TPPS^{-2} in water (pH 3.0), (B) hollow $(PAH/PSS)_2PAH$ and (C) core−shell $CaCO_3$ $(PAH/PSS)_2PAH$ PECs after H_4TPPS^{-2} adsorption (pH 3.0), (D) magnification of image C, (E) Fluorescence lifetime histograms of H_4TPPS^{-2} in water, in hollow and core−shell PECs λexc = 483 nm.

The experimental data obtained for the $CaCO_3$ polyelectrolyte microcapsules holds the hypothesis of a mechanistic pathway with active core influence: the absence of J-aggregates in hollow PECs with the same architecture of core-shells, the higher encapsulation efficiency of core-shells and the low affinity of H_4TPPS^{-2} for $CaCO_3$ cores in the absence of polyelectrolytes. The absence of j-aggregates in the supernatant solution excludes also the possibility of that the needlelike structures are formed in solution and then adsorbed onto the $CaCO_3$ polyelectrolyte microcapsules.

ii. pH 1.5

The pH value of the adsorption solution was decreased to 1.5. J-aggregates formation has already been reported in aqueous solution for pH values near 1 [72] and also the polyelectrolyte complex permeability increases near this value due to the protonation of sulfonate groups of PSS. This mutual effect should improve the conditions for J-aggregation on PECs. All other experimental conditions were kept constant.

Firstly, UV-vis absorption spectroscopy was used in order to check the presence of characteristic J-aggregate bands. In this case, J-aggregation occurs at a lesser extent thus it seems that lowering the pH value of the adsorption solution hinders aggregation phenomena.

The FLIM images of polyelectrolyte microcapsules after H_4TSPP^{-2} adsorption (pH 1.5) obtained at excitation of 650nm reveals high levels of heterogeneity in the microcapsule morphology: rounded shaped and matrix type microcapsules and other irregular structures (Figure 38 (B),(C)) The FLIM images of rounded shaped microcapsules (Figure 38) have an average of 0.5ns which is in agreement with the fluorescence lifetimes obtained for J-aggregates of H_4TSPP^{-2} at pH 0.5. Although there is a confirmed formation of J-aggregates in polyelectrolyte microcapsules at pH 1.5, the formation of needlelike radially distributed structures is not observed in the FLIM images.

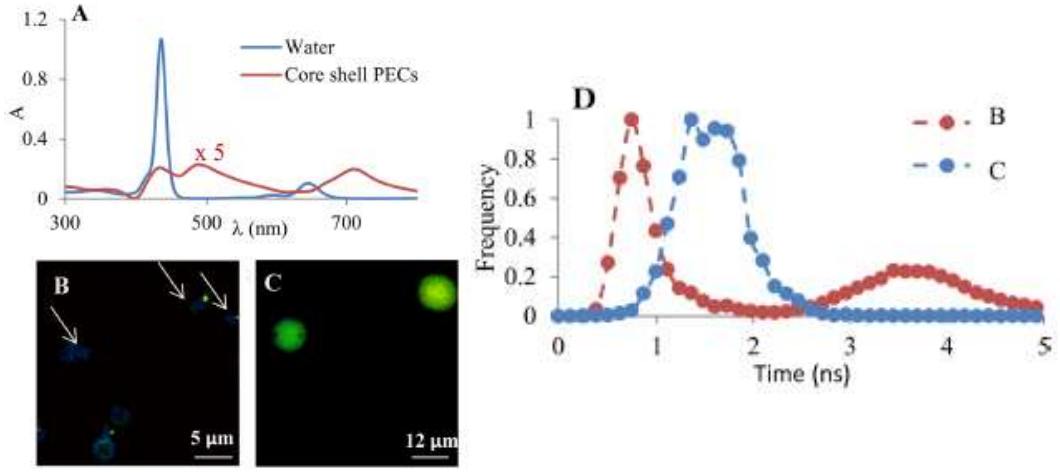

Figure 38 – UV-Vis absorption spectra of H_4TSPP^{-2}in water (pH 1.5) and adsorbed in core-shell $CaCO_3$ $(PAH/PSS)_2PAH$ (A), FLIM images of H_4TSPP^{-2} adsorbed onto $CaCO_3$ $(PAH/PSS)_2PAH$ core-shell at pH1.5 (B,C) and respective fluorescence lifetime histograms of $CaCO_3$ $(PAH/PSS)_2PAH$ (D) The arrows indicate the presence of irregular H_4TSPP^{-2} structures.

Nevertheless, it is possible that the growth of J-aggregates is hindered and only forms nanostructures shorter in length and beyond microscope limit. This can occur due to the increase of ionic strength due to core dissolution.

When the pH value of the adsorption solution is lowered there is a direct impact on ion pair dissociation because the negative charge of PSS is decreased and the positive charge of PAH is maintained. The result of these changes in the polyelectrolytes complex interactions increases the mobility and its network reorganizes itself to form thermodynamically stable complexes.

Also, at low pH values, the $CaCO_3$ cores start to dissolve which causes oscillating inflating-deflating circles due to CO_2 formation and release. The consequence of this effect can be the capsule total collapse or the formation of irregularly shaped microstructures.

iii. Replacement of the polyelectrolyte last layer

According to experimental results of H_4TSPP^{-2} interaction with polyelectrolytes in aqueous solution, the formation of J-aggregates was found to overcome electrostatic repulsion for 20μM PSS solutions. By this reason, PAH last layer was replaced by PSS and the aggregation of H_4TSPP^{-2} in $CaCO_3$ $(PAH/PSS)_2$ was studied whilst maintaining the concentration of the adsorption solution.

An important effect on the optical properties of the adsorbed H_4TSPP^{-2} was found. Besides the presence of J-aggregates characteristic absorption bands, the formation of a new species characterized by an adsorption band at 424 nm is a very interesting result. The characteristic low encapsulation efficiency of hollow polyelectrolyte microcapsules with the same polyelectrolyte complex network may cover for the absence of this band in its respective UV-vis absorption spectrum (Figure 39).

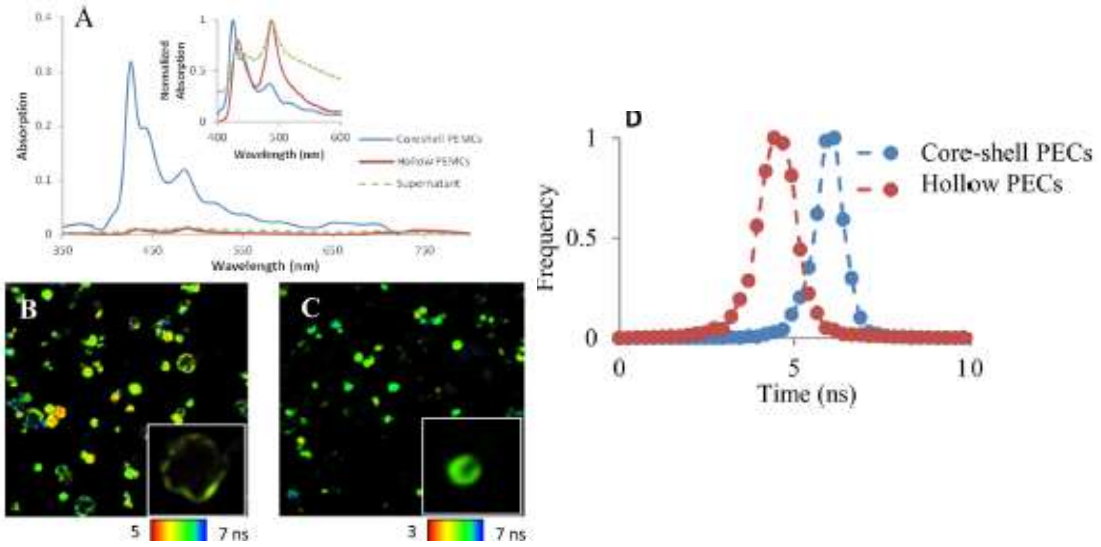

Figure 39 – UV-Vis absorption spectrum (A), FLIM images (80 × 80 μm2) (B,C) and respective fluorescence lifetime histograms of hollow and core-shell $(PAH/PSS)_2$ after adsorption of H_4TSPP^{-2} at pH 1.5 (D)

The presence of similar absorption bands with a similar shape and a bathochromic/hypsochromic shift when compared with the neutral monomeric H_2TSPP^{-4} form has already been studied [73]. However, it is still a subject of some controversy due to its assignment to the presence of H-aggregates or to the short-range aromatic-aromatic interactions between the H_2TSPP^{-4} and the aromatic groups of complementary positive polymers. It is the last hypothesis that is established in the scientific community. [73]

Other results obtained by the group are going to be discussed now. These results are important for further comprehension of the system and the results obtained in several experiments.

c. Interaction of H_4TSPP^{-2} with polyelectrolytes PAH and PSS.

The combination of positive charged porphyrins and negative polyelectrolytes can give rise to the formation of a variety of nanoscale assemblies driven by either electrostatic of π−π interactions [74]. Previous works, by the group and others, have already described the interactions of *meso*-tetraaryl porphyrins (with pH close to neutrality) with PAH and PSS in order to understand the porphyrin interactions within polyelectrolyte hollow microcapsules [47,60].

The porphyrin diacidic form H_4TSPP^{-2} was the chosen structural monomer unit for the porphyrin aggregation within the polyelectrolyte microcapsules. It is important to understand the interactions that occur between this porphyrin dianionic form and polyelectrolytes.

To achieve these different solutions of H_4TSPP^{-2} at a fixed concentration (3 μM) containing variable concentrations of polyelectrolytes were analyzed by UV-vis absorption and fluorescence at pH 3.0 and pH 1.5. The interaction of H_4TSPP^{-2} with PAH and PSS at acidic pH values is very different from the ones reported at pH 6.5. At pH 6.5, H_4TSPP^{-2} absorption spectrum presents a typical band of H-aggregates at [PAH]= 200 μM as shown by the appearance of a hypsochromic shift of the Soret peak. The emission spectrum of this system, it has a bathochromic shift from 644 nm to 665 nm and from 704 nm to 727 nm.

At pH 3.0 and low [PAH] (0.33 μM), the typical spectrum of H_4TSPP^{-2} is replaced by a combination of H-aggregates and J-aggregates characteristic bands. Increasing the [PAH] induces an increase in the J-aggregates characteristic band while reducing the H aggregates and diacid bands (Figure 40A). In the emission spectra, it is only observable the typical monomer bands which can be a result of a residual diacid monomer that has a fluorescence quantum yield higher than the aggregates. The J-aggregates bands are also well observed in the absorption and emission spectra in diacid solutions with increasing concentrations of PSS (Figure 40B). The absorption spectrum has a 3 nm bathochromic shift relatively to the diacid free base spectrum. Also, a noticeable increase of the J-aggregates characteristic bands is found at [PSS] = 20 μM, that tends to decrease at higher polyelectrolyte concentrations. When the [PSS] is high enough that the band at 490nm makes the higher contribution, the emission spectra also changes. It shows an intense band at 710 nm that tends to decrease at higher [PSS]. With [PSS] increase is possible to infer that the balance between hydrophobic and electrostatic interactions change and J aggregation becomes less favorable.

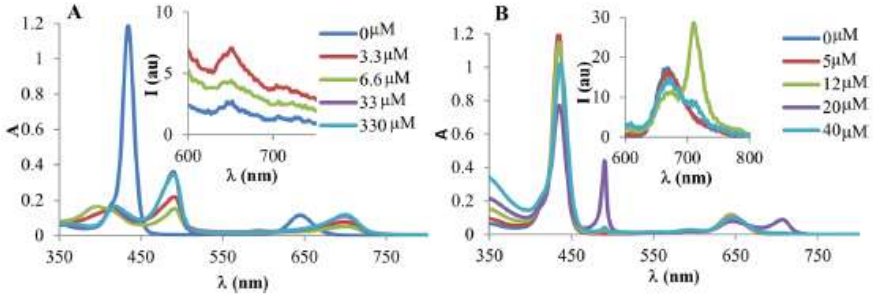

Figure 40 – UV-Vis absorption (A,B) and emission spectra (insets) of H_4TSPP^{-2} (3 μM, pH 3.0, water, rt) with increasing concentrations of PAH (A) and PSS (B). λ_{exc} = 490 nm.

The Fluorescence decays were also obtained for the diacid H_4TSPP^{-2} monomer in the presence of increasing concentration of polyelectrolytes. Using excitation wavelengths of 445 nm and emission wavelength of 650 nm and 710 nm the existence of different species was also predicted whose pre-exponential values are very variable. In solution with the PAH polyelectrolyte, the fluorescence decays are fitted by a triexponential function. The short-lived component can be assigned to the porphyrin aggregates and the intermediate component can be assigned to the diacid porphyrin which is the only one that is obtained in the free diacid H_4TSPP^{-2} solution (water, τ = 3.7 ns). The long-lived component may correspond to a complex formed and mediated by electrostatic interactions between the porphyrin and polyelectrolyte which can also explain the enlargement of the 490nm band owing to superposition with the J aggregate band (Figure 40A). This can be caused due to the acidic pH values with the polyelectrolyte amino groups fully protonated.

Table 9 - Fluorescence Lifetimes of H_4TSPP^{-2} (3 μM, pH 3.0) in Aqueous Solutions with Increasing amounts of Polyelectrolytes

	C (μM)	τ_1 (ns)	A_1 (%)	τ_2 (ns)	A_2 (%)	τ_3 (ns)	A_3 (%)	X^2
PAH	3.3	4.4	16.2	12.1	76.9	<0.5	6.9	1.11
	6.6	4.2	19.6	11.8	72.2	<0.5	8.2	1.12
	33 (a)	3.5	49.7	10.6	33.8	<0.5	16.6	1.04
	(b)	3.6	56.2	10.8	36.3	<0.5	7.5	1.05
	330 (a)	3.1	91.3	-	-	<0.5	8.7	1.28
	(b)	3.1	69.9	10.9	0.7	<0.5	29.4	1.25
PSS	5 (a)	3.8	100	-	-	-	-	1.33
	(b)	3.9	90.3	11.0	0.6	<0.5	9.1	1.27
	12 (a)	3.7	99.4	11.0	0.6	-	-	1.03
	(b)	3.7	98.4	11.0	1.6	-	-	1.22
	20 (a)	3.6	98.6	11.0	1.4	-	-	1.05
	(b)	3.6	97.4	11.0	2.5	-	-	1.19
	40 (a)	3.7	96.6	11.0	3.4	-	-	1.18
	(b)	3.7	96.7	11.0	3.3	-	-	1.23

(a)λ_{em} = 650 nm. (b)λ_{em} = 710 nm.

The presence of the polyelectrolyte in solution can be noticed by a continuous decrease in the fluorescence lifetimes accompanied with an increase in the contributions of the short and intermediate components at the cost of the long-lived pre-exponential factor (table 9). Regarding the H_4TSPP^{-2} interaction with PSS, this effect is less notorious and the formation of J-aggregates is less favored when compared with interaction with the opposite charge polyelectrolyte. Similar interactions have been found at pH 1.5.

The combination between the diacid H_4TSPP^{-2} with polyelectrolytes regardless of their charge, leads to the formation of porphyrin assemblies ruled by electrostatic and π−π interactions. J-aggregates formed in PAH are more stable at higher polyelectrolyte concentrations when comparing with PSS. Nevertheless, pH is still a key factor that controls the H or J aggregation.

The sole interaction of H_4TSPP^{-2} and $CaCO_3$ promotes the formation of J-aggregates due to the presence of characteristic band at 708nm (figure 41). Nevertheless, this interaction is not stable as after a few minutes this band disappears (figure 41 B). This shows that the $CaCO_3$ core may have an inductive j-aggregation effect.

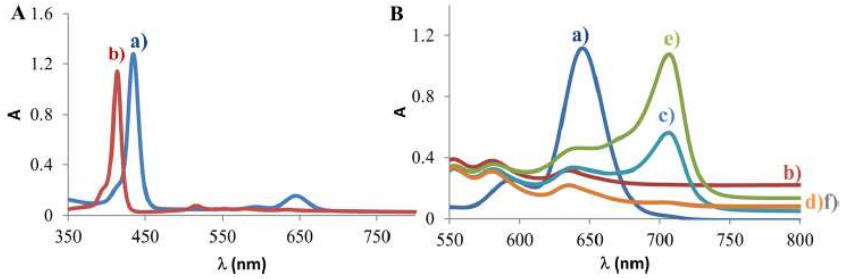

Figure 41 – UV-Vis absorption spectra of H_4TSPP^{-2} (3 μM) in water solutions and in the presence of $CaCO_3$ (A,B). Variations in the absorption spectra of H_4TSPP^{-2} (15 μM) in water solutions (a) in the presence of $CaCO_3$ (b) and with increasing concentrations of H_4TSPP^{-2}: (c) 22 μM, (d) 22 μM after 5 min, (e) 30 μM, and (f) 30 μM after 5 min

d. Following of J aggregation pathway on Core-shells by FLIM

Figure 41 presents the FLIM images and the corresponding average fluorescence lifetime distributions obtained from samples removed from the solution whilst the aggregation on the core-shells was occurring (15 min, 3 hours and 24 hours after porphyrin addition). The formation of the needlelike radiatially distributed J-aggregates is believed to have three fundamental steps: porphyrin adsorption in the polyelectrolyte shell and inorganic core (figure 42A), followed by stabilization of the porphyrin released from the core and its capture by the polyelectrolyte complex network (Figure 42B) which increases local H_4TSPP^{-2} concentration within the shell ending with aggregates growth (Figure 42C).

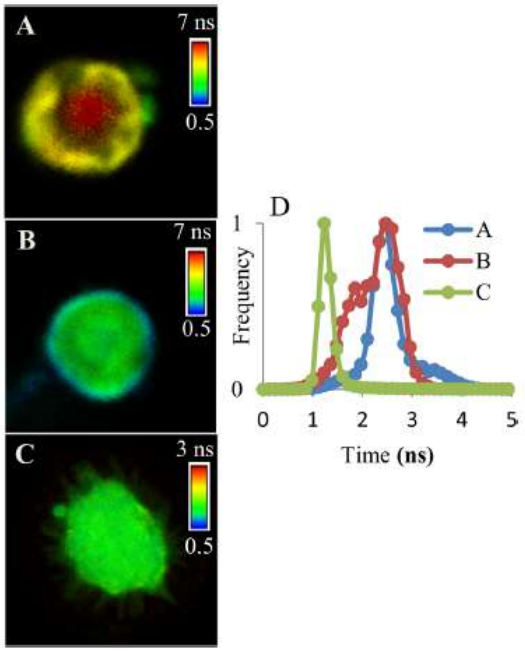

Figure 42 - FLIM images (A−C) and respective fluorescence lifetime histograms (D) of a $CaCO_3$ $(PAH/PSS)_2$ PAH polyelectrolyte microcapsules (A) 15 min, (B) 3 h, and (C) 24 h after H_4TPPS^{-2} addition.

The fluorescence lifetime images allow to distinguish two different domains: nucleus with a 3−5 μm, agreeing with the $CaCO_3$ core structure and that associates longer-lifetime components (τ_{avrg} = 7.2 ns). The polyelectrolyte shell has associated shorter lifetime components (τ_{avrg} = 4.1 ns). Fluorescence lifetimes obtained with point-by-point measurements of the two sections reveal very different decay distribution. In the polyelectrolyte shell, the fluorescent decays are fitted with a biexponential function revealing a shorter component (τ = 2.3ns) and a longer component (τ = 7.4ns) although with lower pre-exponential factor (35%). In the polyelectrolyte core, a biexponential fitting is also done but reveals a shorter component of τ = 3.5 ns and a longer component of τ = 10.3 ns, with balanced preexponential factors (46% and 54%, respectively). The shorter component is very close to the fluorescence lifetimes obtained in water for H_4TSPP^{-2} and the longer components are similar to the fluorescence lifetimes obtained for H_2TSPP^{-4}. In fact, the presence of these two components reveals a different pH values inside the polyelectrolyte microcapsule microenvironment.

After the three hours of adsorption, the two domains easily observed before, cannot be distinguished any longer due to a reorganization of the porphyrin within the core-shell, visible the decrease in the average fluorescence lifetimes. This is more evident after twenty-four hours in which the appearance of needle like structures radially distributed around the polyelectrolyte microcapsule. Fluorescence lifetimes obtained with point-by-point within the microcapsules structure are now comparable and fitted by a triexponential function with a very short lifetime as the main component (80%).

e. Other Results

Although we have already shown that the formation of J-aggregates occurs in polyelectrolyte microcapsules when H_4TSPP^{-2} is adsorbed at pH 3.0 we found interesting to test another methodology and study the effect of the pH in previously adsorbed tetraanionic H_2TSPP^{-4}. In such a way a solution of H_2TSPP^{-4} and 0.6M of KCl is adsorbed at pH 11.0 on polyelectrolyte microcapsules with a last layer of PAH and then the pH is lowered to 1.2, 1.5, 4.0 and 5.5 by emerging them into a water solution at these pH values. By using this methodology, it is expected to form the aggregates precursor (H_4TSPP^{-2}) at lower pH values (1.2, 2.5 and 4) followed by aggregation *in situ.*

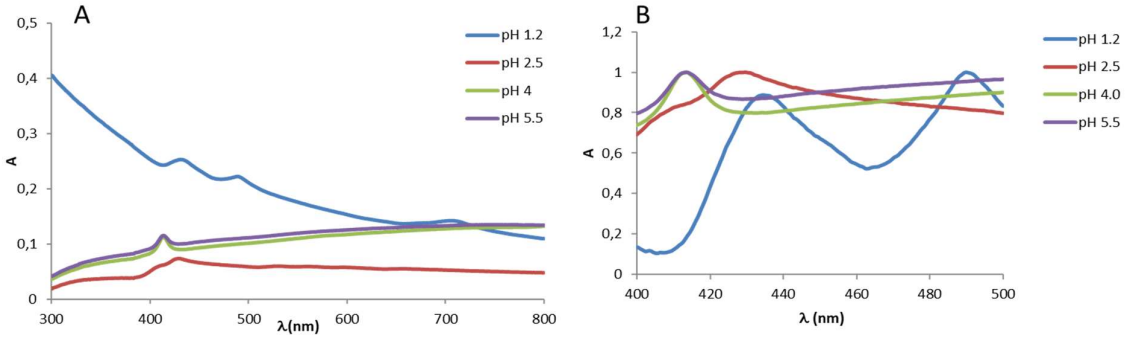

Figure 43– UV-Vis absorption spectra of H_4TSPP^{-2} in core shells $CaCO_3$ $(PAH/PSS)_2$ PAH at different pH values (1.2, 2.5, 4.0 and 5.5). (A) Uncorrected. (B) Normalized

The UV-Vis absorption spectra presented in figure 43 shows that at pH 4.0 and 5.5, H_2TSPP^{-4} is the only form adsorbed on polyelectrolyte microcapsules, noticeable by the Soret band present at 413 nm. At pH 2.5 a band at 428 nm is present but a J-aggregate band (490 nm and 708 nm) is not present. Only at pH 1.2, the porphyrin J aggregation occurs, as the characteristic J-aggregate band is present along with the Soret band of H_4TSPP^{-2} (434nm). Fluorescence lifetime imaging microscopy was used to verify the presence of J-aggregates.

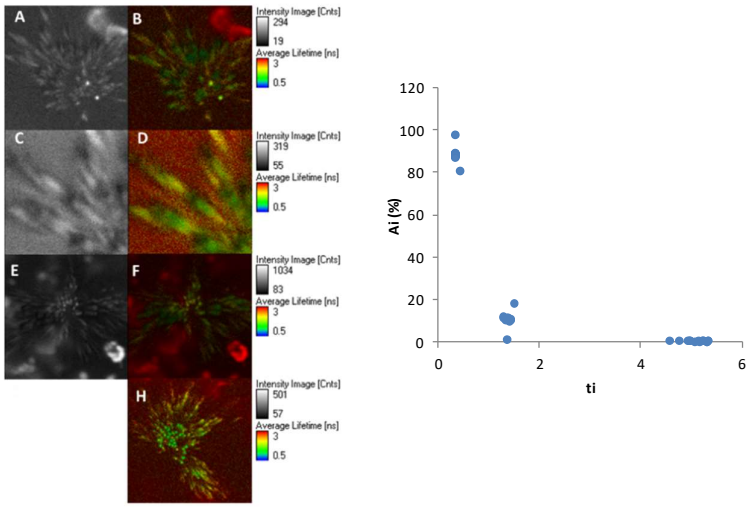

Figure 44 – FLIM images and fluorescence lifetime distribution of PECs with TSPP adsorbed at pH 1.2. λ_{exc}=483 nm

In figure 44, is presented the FLIM images and the distribution of lifetimes collected from the system formed at pH 1.2.

Compared with the already discussed polyelectrolyte microcapsule system with H_4TSPP^{-2} adsorbed at pH 3.0 (figure 37), the J-aggregates formed by this methodology have a bigger size and although they are not as uniformly distributed around the microcapsule, as the other system, it still presents needle like structures radially distributed around the microcapsule surroundings. Nevertheless, the presence of a background signal with a longer lifetime (τ ~ 3.8 ns) is similar to H_4TSPP^{-2} in glass. Is possible to predict that the release of the porphyrin from the polyelectrolyte microcapsules occurs prior to J-aggregates formation, favoring aggregation outside the microcapsule structure.

The fluorescence lifetime presents an accordance with the formation of J-aggregates as the decomposition of fluorescence lifetimes in a third part exponential decay, obtained by time-resolved fluorescence emission, reveals a bigger contribution of the shorter lifetime factor correspondent with the present of H_4TSPP^{-2} J-aggregates.

This methodology instead of promoting the formation of J-aggregates in the polyelectrolyte microcapsule structure, as the one described in chapter 6, it promotes the formation of J-aggregates in solution (at a lower pH value) using polyelectrolyte microcapsules as a reservoir where are deposited and arranged and not as a nucleation site.

f. Conclusions and potential applications

With this work, a simple, fast and scalable new methodology to prepare photoactive core-shell polyelectrolyte microcapsules containing porphyrin aggregates was successfully developed, via combination of a diacid porphyrin H_4TSPP^{-2} at pH 3.0, an inorganic core $CaCO_3$ and a pH sensitive polyelectrolyte complex (PSS/PAH). Spherical core-shell microcapsules functionalized with radially distributed porphyrin self-assembled needles sticking out were viewed by FLIM.

The existence of a core and polyelectrolyte cooperative and synergistic effect supports the results obtained. The directional growth is also proposed as it starts by the porphyrin adsorption in the polyelectrolyte microcapsule followed by stabilization of the porphyrin release from the core and captured by the polyelectrolyte complex and ending with the aggregate growth due initiated by the increase in the local porphyrin concentration.

Lower than pH 3.0, the polyelectrolyte microcapsules become unstable and the core-shell collapse is possible. Changing the last layer from PAH to PSS has also a negative outcome in the J-aggregates formation.

As it was already stated in the introductory section of this chapter, the photodynamic activity of J-aggregates is low due to significant reduction of the intersystem crossing yield, leading to low triplet state efficiencies. However, J-aggregates are an efficient model that mimics light-harvesting systems and supports faster energy transport due to its strong intermolecular coupling. To this, J-aggregates present themselves as organic system with optoelectronics applications.

The absorption characteristic peak at 490 nm is near the maximum spectral irradiance wavelength of electromagnetic radiation coming from the sun. This way, one of the possible applications is its incorporation as a light-harvesting system in an organic solar cell with a neighboring cathode and anode coupled with an electron acceptor. Other applications are also dependent on the characteristic sharp absorption band of J-aggregates as it can be incorporated in the design on specific photodiodes with the detection capacity up to two different wavelengths (two higher peaks at 490nm and 708nm) [75,76].

CHAPTER 7

General Conclusions and Future Remarks

In this work, polyelectrolyte microcapsules with potential applications in PDT were prepared and further knowledge of PEC system adsorbed with porphyrins was obtained. For the use in PDT, adsorption of porphyrin was conducted on polyelectrolyte microcapsules. Photosensitizer photochemical properties were studied and analyzed revealing different characteristics depending on the environment, sole interaction with polyelectrolytes and adsorbed on polyelectrolyte microcapsules. The drug loading, encapsulation efficiency and drug release were measured showing different values according to polyelectrolyte microcapsules architecture and environment pH: a neutral pH environment showed a high stability of the system whereas acidic pH environment promoted a high release of therapeutic cargo. The systems were also characterized by time-resolved fluorescence and fluorescence lifetime imaging (FLIM).

The system designed $CaCO_3$ $(PAH/PSS)_2PAH$ revealed a drug release of almost 90% of its initial cargo in five hours at an acidic pH being the most promising system for use in stomach cancer therapy. It is therefore important as future work to increase the potential therapeutic effect of the system. One way to achieve this is to take advantage of pathological characteristics of the disease such as enhanced permeability and retention of macromolecules and porphyrinoids (EPR) where the physicochemical properties of the delivery system has a major role. If porphyrin functionalization is not enough to guarantee tumor selective and specificity, polyelectrolyte microcapsules surface modification must be considered. Adsorption of PEG or the use of thiol groups or thiomers can be done in order to increase systemic circulation and accumulation of the system in the target area. In the case of thiol group modification, it increases the adherence through covalent binding to the fluid mucus layer of the stomach. Another way, is to actively target a specific tumor. For this, surface or polyelectrolyte modification should be done with the use of aptamers or immunoglobulins that target over-expressed molecules or membrane receptors. In the case of gastric cancer promoted by *helicobacter pylori* infection, IFNγ is over-expressed making it a suitable target also, for targeting of this gram-negative bacterium is better suited the use of a cationic photosensitizer such as TMPyP. Another way to increase the potential therapeutic effect of this system is by increasing singlet oxygen quantum yield. Porphyrin chemical modification, as the introduction of halogens as substituents or metal coordination should increase intersystem crossing by spin-orbiting coupling interaction.

Additionally, and during the experimental work developed in the aim of the project objectives, we have also found interesting conditions to promote the aggregates growth on these systems. Although porphyrin aggregates are non-ideal structures to cancer therapeutics, other interesting applications can be found. In such a way, it is also reported herein a new methodology to obtain photoactive core−shell polyelectrolyte microcapsules containing porphyrin aggregates with radially distributed porphyrin self-assembled needles, sticking out of the microcapsule shell as confirmed by fluorescence lifetime imaging microscopy (FLIM).

Bibliography

[1] J. Ferlay, I. Soerjomataram, R. Dikshit, S. Eser, C. Mathers, M. Rebelo, D.M. Parkin, D. Forman, F. Bray (2014). Cancer incidence and mortality worldwide: sources, methods and major patterns in GLOBOCAN 2012. International Journal of Cancer.

[2] Vergaro, V., Scarlino, F., Bellomo, C., Rinaldi, R., Vergara, D., Maffia, M., Baldassarre, F., Giabbelli, G., Zhang, X., Lvol, Y., Leporatti, S. (2011). Drug-loaded polyelectrolyte microcapsules for sustained targeting of cancer cells. *Advanced Drug Delivery Reviews*, *63*(9), 847–864.

[3] Jabr-Milane, L. S., van Vlerken, L. E., Yadav, S., Amiji, M. M. (2008). Multi-functional nanocarriers to overcome tumor drug resistance. *Cancer Treatment Reviews*, *34*(7), 592–602.

[4] Moghimi, S. M., Hunter, A. C., J.C. Murray. (2005). Nanomedicine: current status and future prospects. *The FASEB Journal*, *19*(3), 311–330.

[5]Schneider, L. A., Hinrichs, R., Scharffetter-Kochanek, K. (2008). Phototherapy and photochemotherapy. *Clinics in Dermatology*, *26*(5), 464–476.

[6] Valko, M., Leibfritz, D., Moncol, J., Cronin, M. T., Mazur, M., Telser, J. (2007). Free radicals and antioxidants in normal physiological functions and human disease. *The International Journal of Biochemistry & Cell Biology*, *39*(1), 44–84.

[7] Rahman, T., Hosen, I., Islam, M. M. T., Shekhar, H. U. (2012). Oxidative stress and human health. *Advances in Bioscience and Biotechnology*, *3*(7), 997–1019.

[8] Sudhakara, R., Ramya, K., Ramesh, T., Gudapati, S., Madhavai, S., Kiran, S. (2012). Photodynamic Therapy in Oral Diseases. *International Journal of Biological & Medical Research*, *3*(2), 1875–1883.

[9] Oniszczuk, A., Wojtunik-Kulesza, K. A., Oniszczuk, T., Kasprzak, K. (2016). The potential of photodynamic therapy (PDT)—Experimental investigations and clinical use. *Biomedicine & Pharmacotherapy*, *83*, 912–929.

[10] Kasha, M. (1950). Characterization of electronic transitions in complex molecules. *Discussions of the Faraday Society*, *9*(c), 14-19.

[11] Lakowicz, J. R. (2006). *Principles of Fluorescence Spectroscopy*. (J. R. Lakowicz, Ed.), *Principles of fluorescence spectroscopy, Springer, New York, USA, 3rd edn, 2006.* Boston, MA: Springer US.

[12] Stokes, G. G. (1852). On the Change of Refrangibility of Light. *Philosophical Transactions of the Royal Society of London*, *142*, 463–562.

[13] Bonnett, R. (1995). Photosensitizers of the porphyrin and phthalocyanine series for photodynamic therapy. *Chemical Society Reviews*, *24*(1), 19-33.

[14] Webb, L. E., Fleischer, E. B. (1965). Crystal Structure of Porphine. *The Journal of Chemical Physics*, *43*(9), 3100–3111.

[15] Gottfried, J. M. (2015). Surface chemistry of porphyrins and phthalocyanines. *Surface Science Reports*, *70*(3), 259–379.

[16] L.R. Milgrom, (1997). The Colors of Life: An Introduction to the Chemistry of Porphyrins and Related Compounds. Oxford University Press.

[17] Hollingsworth, J. V, Richard, A. J., Vicente, M. G. H., Russo, P. S. (2012). Characterization of the Self-Assembly of *meso* -Tetra(4-sulfonatophenyl)porphyrin (H 2 TPPS 4–) in Aqueous Solutions. *Biomacromolecules*, *13*(1), 60–72.

[18] Lauceri, R., De Napoli, M., Mammana, A., Nardis, S., Romeo, A., Purrello, R. (2004). Hierarchical self-assembly of water-soluble porphyrins. *Synthetic Metals*, *147*(1–3), 49–55.

[19] Serra, V. V., Teixeira, R., Andrade, S. M., Costa, S. M. B. (2016). Design of polyelectrolyte core-shells with DNA to control TMPyP binding. *Colloids and Surfaces B: Biointerfaces*, *146*(May), 127–135.

[20] Rainò, G., Stöferle, T., Park, C., Kim, H.-C., Chin, I.-J., Miller, R. D., Mahrt, R. F. (2010). Dye Molecules Encapsulated in a Micelle Structure: Nano-Aggregates with Enhanced Optical Properties. *Advanced Materials*, *22*(33), 3681–3684.

[21] Reddi, E., Ceccon, M., Valduga, G., Jori, G., Bommer, J. C., Elisei, F., Latterini, L., Mazzucato, U. (2002). Photophysical properties and antibacterial activity of meso-substituted cationic porphyrins. *Photochemistry and Photobiology*, *75*(5), 462–70.

[22] Snyder, J. W., Lambert, J. D. C., Ogilby, P. R. (2006). 5,10,15,20-Tetrakis(N-Methyl-4-Pyridyl)-21H,23H-Porphine (TMPyP) as a Sensitizer for Singlet Oxygen Imaging in Cells: Characterizing the Irradiation-dependent Behavior of TMPyP in a Single Cell. *Photochemistry and Photobiology*, *82*(1), 177-184.

[23] Jiménez-Banzo, A., Sagristà, M. L., Mora, M., Nonell, S. (2008). Kinetics of singlet oxygen photosensitization in human skin fibroblasts. *Free Radical Biology and Medicine*, *44*(11), 1926–1934.

[24]National Center for Biotechnology Information. PubChem Compound Database; CID=482745, https://pubchem.ncbi.nlm.nih.gov/compound/482745.

[25] Rosa, A., Ricciardi, G., Baerends, E. J. (2006). Synergism of Porphyrin-Core Saddling and Twisting of *meso* -Aryl Substituents. *The Journal of Physical Chemistry A*, *110*(15), 5180–5190.

[26] Vaz Serra, V., Neto, N. G. B., Andrade, S. M., Costa, S. M. B. (2017). Core-Assisted Formation of Porphyrin J-Aggregates in pH-Sensitive Polyelectrolyte Microcapsules Followed by Fluorescence Lifetime Imaging Microscopy. *Langmuir*, *33*(31), 7680–7691.

[27] Andrade, S. M., Costa, S. M. B. (2008). Ordered Self-assembly of Protonated Porphyrin Induced by the Aqueous Environment of Biomimetic Systems. *Annals of the New York Academy of Sciences*, *1130*(1), 305–313.

[28] Gonalves, P. J., Franzen, P. L., Correa, D. S., Almeida, L. M., Takara, M., Ito, A. S., Zílio, S. C., Borissevitch, I. E. (2011). Effects of environment on the photophysical characteristics of mesotetrakis methylpyridiniumyl porphyrin (TMPyP). *Spectrochimica Acta - Part A: Molecular and Biomolecular Spectroscopy*, *79*(5), 1532–1539.

[29] Kataoka, K., Harada, A., Nagasaki, Y. (2001). Block copolymer micelles for drug delivery: design, characterization and biological significance. *Advanced Drug Delivery Reviews*, *47*(1), 113–131.

[30] Madene, A., Jacquot, M., Scher, J., Desobry, S. (2006). Flavour encapsulation and controlled release - a review. *International Journal of Food Science and Technology*, *41*(1), 1–21.

[31] Tsuji, K. (2001). Microencapsulation of pesticides and their improved handling safety. *Journal of Microencapsulation*, *18*(2), 137–147.

[32] Ammala, A. (2013). Biodegradable polymers as encapsulation materials for cosmetics and personal care markets. *International Journal of Cosmetic Science*, *35*(2), 113–124.

[33] Nelson, G. (2002). Application of microencapsulation in textiles. *International Journal of Pharmaceutics*, *242*(1–2), 55–62.

[34] Akers Jr CE, Sun XJ. Encapsulated pigment for ink-jet ink formulations and methods of producing same. United States Patent Office, US7354962 B1; 2008 Lexmark International, Inc. Lexington, KY, US.

[35] Park, B.-W., Yoon, D.-Y., Kim, D.-S. (2010). Recent progress in bio-sensing techniques with encapsulated enzymes. *Biosensors and Bioelectronics*, *26*(1), 1–10.

[36] Shchukin, D. G., Grigoriev, D. O., Möhwald, H. (2010). Application of smart organic nanocontainers in feedback active coatings. *Soft Matter*, *6*(4), 720–725.

[37] Raj, V. A. A., Velraj, R. (2010). Review on free cooling of buildings using phase change materials. *Renewable and Sustainable Energy Reviews*, *14*(9), 2819–2829.

[38] Peyratout, C. S., Dähne, L. (2004). Tailor-Made Polyelectrolyte Microcapsules: From Multilayers to Smart Containers. *Angewandte Chemie International Edition*, *43*(29), 3762–3783.

[39] Sukhorukov, G. B., Volodkin, D. V., Günther, A. M., Petrov, A. I., Shenoy, D. B., Möhwald, H. (2004). Porous calcium carbonate microparticles as templates for encapsulation of bioactive compounds. *Journal of Materials Chemistry*, *14*(14), 2073–2081.

[40] Johnston, A. P. R., Cortez, C., Angelatos, A. S., Caruso, F. (2006). Layer-by-layer engineered capsules and their applications. *Current Opinion in Colloid & Interface Science*, *11*(4), 203–209.

[41] Sigma-Aldrich Catalog. http://www.sigmaaldrich.com/catalog/AdvancedSearchPage.do. Product Number – 283223 AND 561223

[42] Márquez-Beltrán, C., Castañeda, L., Enciso-Aguilar, M., Paredes-Quijada, G., Acuña-Campa, H., Maldonado-Arce, A., Argillier, J.-F. (2013). Structure and mechanism formation of polyelectrolyte complex obtained from PSS/PAH system: effect of molar mixing ratio, base–acid conditions, and ionic strength. *Colloid and Polymer Science*, *291*(3), 683–690.

[43] Ai, H., Pink, J. J., Shuai, X., Boothman, D. A., Gao, J. (2005). Interactions between self-assembled polyelectrolyte shells and tumor cells. *Journal of Biomedical Materials Research Part A*, *73A*(3), 303–312.

[44] Fischlechner, M., Zschörnig, O., Hofmann, J., Donath, E. (2005). Engineering Virus Functionalities on Colloidal Polyelectrolyte Lipid Composites. *Angewandte Chemie International Edition*, *44*(19), 2892–2895.

[45] Cheng, L., Yang, K., Chen, Q., Liu, Z. (2012). Organic Stealth Nanoparticles for Highly Effective *in Vivo* Near-Infrared Photothermal Therapy of Cancer. *ACS Nano*, *6*(6), 5605–5613.

[46] Cortez, C., Tomaskovic-Crook, E., Johnston, A. P. R., Scott, A. M., Nice, E. C., Heath, J. K., Caruso, F. (2007). Influence of Size, Surface, Cell Line, and Kinetic Properties on the Specific Binding of A33

Antigen-Targeted Multilayered Particles and Capsules to Colorectal Cancer Cells. *ACS Nano*, *1*(2), 93–102.

[47] Bédard, M. F., Sadasivan, S., Sukhorukov, G. B., Skirtach, A. (2009). Assembling polyelectrolytes and porphyrins into hollow capsules with laser-responsive oxidative properties. *Journal of Materials Chemistry*, *19*(15), 2226-2233.

[48] Delcea, M., Möhwald, H., Skirtach, A. G. (2011). Stimuli-responsive LbL capsules and nanoshells for drug delivery. *Advanced Drug Delivery Reviews*, *63*(9), 730–747.

[49] Luo, G.-F., Xu, X.-D., Zhang, J., Yang, J., Gong, Y.-H., Lei, Q., Jia, H.-Z., Li, C., Zhuo, R.-X., Zhang, X.-Z. (2012). Encapsulation of an Adamantane-Doxorubicin Prodrug in pH-Responsive Polysaccharide Capsules for Controlled Release. *ACS Applied Materials & Interfaces*, *4*(10), 5317–5324.

[50] Wu, Z., Lin, X., Zou, X., Sun, J., He, Q. (2015). Biodegradable Protein-Based Rockets for Drug Transportation and Light-Triggered Release. *ACS Applied Materials & Interfaces*, *7*(1), 250–255.

[51] Zelikin, A. N., Quinn, J. F., Caruso, F. (2006). Disulfide Cross-Linked Polymer Capsules: En Route to Biodeconstructible Systems. *Biomacromolecules*, *7*(1), 27–30.

[52] Valeur, B., Berberan-Santos, M. N. (2012). *Molecular Fluorescence*. *Methods* (Vol. 8). Weinheim, Germany: Wiley-VCH Verlag GmbH & Co. KGaA.

[53] Kaszuba, M., Corbett, J., Watson, F. M., Jones, A. (2010). High-concentration zeta potential measurements using light-scattering techniques. *Philosophical Transactions of the Royal Society A: Mathematical, Physical and Engineering Sciences*, *368*(1927), 4439–4451.

[54] Johnson Jr., C. S., Gabriel, D. A. (1995). *Laser Light Scattering*. Dover Publications, Inc., New York.

[55] Smoluchowski, M. von (1914). Studien über Molekularstatistik von Emulsionen und deren Zusammenhang mit der Brown'schen Bewegung. *Sitzungsberichte. Akademie der Wissenschaften*. Mathematisch-Naturwissenschaftliche Klasse. CXXIII Band. X Heft. Dez. 1914. Abteilung II A. Wien. 2381-2405.

[56] GmbH, PicoQuant. "Home." Fluorescence Lifetime Imaging (FLIM) | PicoQuant. Web. 29 Jan. 2017.

[57] Paredes, A. M. (2014). MICROSCOPY | Scanning Electron Microscopy. Encyclopedia of Food Microbiology (Second Edition, Vol. 2). Elsevier.

[58] Cook, M. T., Tzortzis, G., Khutoryanskiy, V. V., Charalampopoulos, D. (2013). Layer-by-layer coating of alginate matrices with chitosan–alginate for the improved survival and targeted delivery of probiotic bacteria after oral administration. *Journal of Materials Chemistry B*, *1*(1), 52–60.

[59] Shavit, N. (1973). Electrical Mobility of Counterions in Polyelectrolyte Solutions. *Israel Journal of Chemistry*, *11*(2–3), 235–242.

[60] Teixeira, R., Serra, V. V., Paulo, P. M. R., Andrade, S. M., Costa, S. M. B. (2015). Encapsulation of photoactive porphyrinoids in polyelectrolyte hollow microcapsules viewed by fluorescence lifetime imaging microscopy (FLIM). *RSC Advances*, *5*(96), 79050–79060.

[61] Gonçalves, P. J., Barbosa Neto, N. M., Parra, G. G., de Boni, L., Aggarwal, L. P. F., Siqueira, J. P., Misoguti, L., Borissevitch, I.E., Zílio, S. C. (2012). Excited-state dynamics of meso-tetrakis(sulfonatophenyl) porphyrin J-aggregates. *Optical Materials*, *34*(4), 741–747.

[62] Gust, D., Moore, T. A., Moore, A. L. (2001). Mimicking Photosynthetic Solar Energy Transduction. *Accounts of Chemical Research*, *34*(1), 40–48.

[63] Valli, L., Casilli, S., Giotta, L., Pignataro, B., Conoci, S., Borovkov, V. V., Inoue, Y., Sortino, S. (2006). Ethane-Bridged Zinc Porphyrin Dimers in Langmuir−Shäfer Thin Films: Structural and Spectroscopic Properties. *The Journal of Physical Chemistry B*, *110*(10), 4691–4698.

[64] Kim, D., Osuka, A. (2004). Directly Linked Porphyrin Arrays with Tunable Excitonic Interactions. *Accounts of Chemical Research*, *37*(10), 735–745.

[65] Eisfeld, A., Briggs, J. S. (2006). The J- and H-bands of organic dye aggregates. *Chemical Physics*, *324*(2–3), 376–384.

[66] Guo, P., Chen, P., Ma, W., Liu, M. (2012). Morphology-dependent supramolecular photocatalytic performance of porphyrin nanoassemblies: from molecule to artificial supramolecular nanoantenna. *Journal of Materials Chemistry*, *22*(38), 20243.

[67] Bera, R., Mandal, S., Mondal, B., Jana, B., Nayak, S. K., Patra, A. (2016). Graphene–Porphyrin Nanorod Composites for Solar Light Harvesting. *ACS Sustainable Chemistry & Engineering*, *4*(3), 1562–1568.

[68] Sadasivan, S., Köhler, K., Sukhorukov, G. B. (2006). Fabrication of Organized Porphyrin-Nanotube-Attached Heat-Sensitive Polyelectrolyte Capsules. *Advanced Functional Materials*, *16*(16), 2083–2088.

[69] Würthner, F., Kaiser, T. E., Saha-Möller, C. R. (2011). J-Aggregates: From Serendipitous Discovery to Supramolecular Engineering of Functional Dye Materials. *Angewandte Chemie International Edition*, *50*(15), 3376–3410.

[70] Seybold, P. G., Gouterman, M. (1969). Porphyrins: XIII: Fluorescence spectra and quantum yields. *Journal of Molecular Spectroscopy*, *31*(1–13), 1–13.

[71] Ohno, O., Kaizu, Y., Kobayashi, H. (1993). J -aggregate formation of a water-soluble porphyrin in acidic aqueous media. *The Journal of Chemical Physics*, *99*(5), 4128–4139.

[72] Fujii, Y., Hasegawa, Y., Yanagida, S., Wada, Y. (2005). pH-Dependent reversible transformation of TPPS4 anchored on mesoporous TiO_2 film between monomers and J-aggregates. *Chemical Communications*, *0*(24), 3065-3067.

[73] Zhao, L., Ma, R., Li, J., Li, Y., An, Y., Shi, L. (2008). J- and H-Aggregates of 5,10,15,20-Tetrakis-(4-sulfonatophenyl)-porphyrin and Interconversion in PEG- b -P4VP Micelles. *Biomacromolecules*, *9*(10), 2601–2608.

[74] Ruthard, C., Maskos, M., Kolb, U., Gröhn, F. (2009). Finite-Size Networks from Cylindrical Polyelectrolyte Brushes and Porphyrins. *Macromolecules*, *42*(3), 830–840.

[75] Jansen-van Vuuren, R. D., Armin, A., Pandey, A. K., Burn, P. L., Meredith, P. (2016). Organic Photodiodes: The Future of Full Color Detection and Image Sensing. *Advanced Materials*, *28*(24), 4766–4802.

[76] Pais, A., Banerjee, A., Klotzkin, D., Papautsky, I. (2008). High-sensitivity, disposable lab-on-a-chip with thin-film organic electronics for fluorescence detection. *Lab on a Chip*, *8*(5), 794-800.

Annexes

Annexes 1 – Encapsulation Efficiency and Drug Loading

The Efficiency Encapsulation for the different systems was calculated by dividing the mass of porphyrin adsorbed by the microcapsule mass weighed [S. Papadimitriou, D. Bikiaris. Journal of Controlled Release 138 (2009) 177–184]. For each system it was done an average of three experiments and calculated the standard deviation between them.

$$Encapsulation\ Efficiency\ (\%) = \frac{Mass\ of\ Porphyrin\ Adsorbed\ (mg)}{Mass\ of\ Microcapsules\ (mg)} \times 100$$

$$Drug\ Loading\ (\%) = \frac{[Porphyrin\ Adsorbed]\ (mg\ ml^{-1})}{[Porphyrin]_0\ (mg\ ml^{-1})} \times 100$$

$$Mass\ of\ Porphyrin\ (g) = Molecular\ Weight\ \left(\frac{g}{mol}\right) \times Porphyrin\ Adsorbed\ (M)$$

Annexes 2 – Environment neutralization

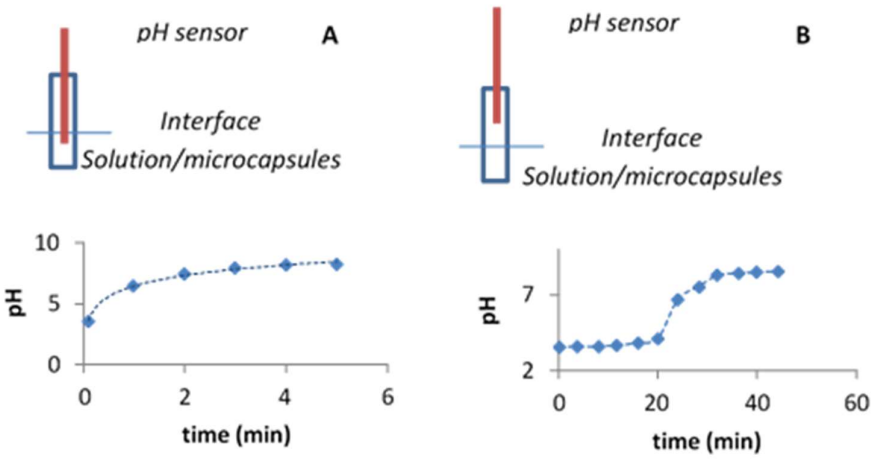

The environment neutralization of core-shells of polyelectrolyte microcapsules is evaluated with a pH sensor along time. The starting medium has a pH of 2.0